MOX–Report No. 37/2012

Exact and inexact partitioned algorithms for fluid-structure interaction problems with finite elasticity in haemodynamics

Nobile, F.; Pozzoli, M.; Vergara, C.

MOX, Dipartimento di Matematica "F. Brioschi"
Politecnico di Milano, Via Bonardi 9 - 20133 Milano (Italy)

mox@mate.polimi.it http://mox.polimi.it

Exact and inexact partitioned algorithms for fluid-structure interaction problems with finite elasticity in haemodynamics*

F. Nobile[1,2], M. Pozzoli[3], C. Vergara[3]

September 13, 2012

[1] MOX– Modellistica e Calcolo Scientifico
Dipartimento di Matematica "F. Brioschi"
Politecnico di Milano
via Bonardi 9, 20133 Milano, Italy

[2] MATHICSE, CMCS, EPF de Lausanne, Switzerland
fabio.nobile@epfl.ch

[3] Dipartimento di Ingegneria dell'Informazione e Metodi Matematici
Università di Bergamo
via Marconi 5, 24044, Italy
matteo1.pozzoli@unibg.it, christian.vergara@polimi.it

Keywords: Fluid-structure Interaction, finite elasticity, partitioned algorithms, Robin transmission conditions, haemodynamics

Abstract

In this paper we consider the numerical solution of the three-dimensional (3D) fluid-structure interaction problem in haemodynamics, in the case of physiological geometries and data, and finite elasticity vessel deformations. We introduce new partitioned algorithms and compare their efficiency with that of existing ones. We also study some new inexact variants, obtained from semi-implicit approximations, and show that they allow to improve the efficiency while preserving the accuracy of the related exact (implicit) scheme.

*This work has been supported by the ERC Advanced Grant N.227058 MATHCARD and by the Italian MIUR PRIN09 project n. 2009Y4RC3B_001.

1 Introduction

To obtain predictive accurate information about the blood fluid-dynamics in the arteries of the cardiovascular tree, it is necessary to solve in three-dimensional (3D) realistic geometries a fluid-structure interaction (FSI) problem, that arises from the interaction between blood and vascular vessel [41, 7, 14, 44, 12, 3, 16, 17].

To capture the complex dynamics, non-linear fluid and structure models have to be taken into account. This leads to the solution of a complex non-linear coupled problem, formed by the fluid and the structure subproblems, together with the fluid domain subproblem when the fluid equations are written in *Arbitrary Lagrangian-Eulerian* (ALE) formulation [25, 11]. Efficient numerical strategies are mandatory to solve such non-linear FSI problem in 3D real geometries and with physiological data. Only few works have focused on this aspect. We mention [7, 34] among the *monolithic schemes*, which build the whole non-linear system, and [30, 21] among the *partitioned schemes*, which consist in the successive solution of the subproblems in an iterative framework (see also [12, 5, 4, 9] in the case of infinitesimal elasticity).

In this work, we focus on the numerical solution of the FSI problem with partitioned strategies in haemodynamics, when non-linear sub-problems and 3D real computational domains and physiological data are considered. This problem is very complex, the main difficulties being:

1. The high *added mass effect*, due to the similar fluid and structure densities, which makes very difficult the solution of the FSI problem with partitioned strategies [8, 20, 40];

2. The treatment of the *physical interface conditions*, which enforce the continuity of velocities and normal stresses at the fluid-structure (FS) interface between the fluid and the structure subproblems;

3. The treatment of the *geometrical interface condition*, which enforces the continuity of displacements at the FS interface between the fluid and the structure domains;

4. The treatment of the *constitutive non-linearities* in the fluid and the structure models.

Regarding points 1 and 2, it has been clearly highlighted in several works that the physical conditions have to be treated implicitly in haemodynamics, due to the high added mass effect [8, 20, 3, 40]. In particular, in this work we consider partitioned algorithms based on Robin interface conditions, which have good convergence properties, independent of the added-mass effect [3, 4, 1, 22, 38].

For what concerns point 3, we can distinguish between exact and inexact algorithms. The first group consists in those schemes that satisfy exactly the geometrical interface condition (*geometrical exact schemes* [23, 7, 13]). On the contrary, in the *geometrical inexact schemes* this condition is not satisfied, due to an explicit treatment of the interface position by extrapolation from previous time steps

(the so-called *semi-implicit* schemes [12, 6, 39]), or to an *a priori* fixed number of "fixed-point" iterations performed over the interface position [38]. The semi-implicit schemes have been shown to be stable [37, 43, 12, 39] and accurate [36, 2] in the case of the linear infinitesimal elasticity.

Regarding point 4, we have to consider the fluid and the structure constitutive non-linearities. We focus here on partitioned strategies, obtained by the application of a suitable linearization of the monolithic system. A first approach of this type consists in solving the non-linear fluid and structure subproblems in an iterative framework until convergence of the physical continuity conditions (think for example to the classical Dirichlet-Neumann scheme) [29, 31, 24, 27, 40]. At each iteration two non-linear subproblems have to be solved, for example with the Newton method. In this case, the constitutive non-linearities are treated in an inner loop with respect to both the physical and the geometrical interface conditions. We refer to these schemes as "classical" partitioned algorithms. A second strategy considered so far consists in applying the Newton or the approximate-Newton method (the latter obtained by approximating the tangent operator) to the monolithic non-linear system (*approximate-Newton-based algorithms*). In [23], the author proposed a block-diagonal approximation of the Jacobian, leading to a partitioned algorithm where all the interface conditions and non-linearities are treated in the same loop (see also [33, 24, 30, 10, 45]). In [38], the authors considered alternative approximations of the Jacobian, leading to different, most efficient partitioned algorithms. The general structure of such schemes consists in an external loop to manage the geometrical interface condition and the constitutive non-linearities and in an internal one to prescribe the physical interface conditions.

The study of the effectiveness and accuracy of different partitioned schemes to treat the structure non-linearity for a full non-linear FSI problem in haemodynamics is far to be exhaustive nowadays. The present work aims at providing some answers in this direction.

The first goal of this paper consists in comparing the performance of different partitioned algorithms, to understand which are the most effective for 3D real haemodynamic applications. In particular, we considered three families of schemes: the "classical" algorithms, the approximate-Newton-based algorithms, a new class of schemes, obtained by considering fixed point iterations over the geometrical interface condition (*fixed-point-based* schemes). For all the three families, we considered several alternatives, all based on the exchange of Robin conditions to prescribe the physical interface conditions. We ran each of the considered scheme on a real 3D geometry with physiological data, with the aim of studying the efficiency of such schemes for practical purposes. The reported numerical results show that the double loop approximate-Newton-based schemes are the most performing, while the classical ones are the slowest.

All the algorithms considered so far solve "exactly" (i.e. up to a given small tolerance) the non-linear FSI problem. As already mentioned earlier, in the context of linear elasticity, semi-implicit approaches which treat explicitly the geometrical coupling have been proven to be stable and accurate. It is therefore worth asking

if in haemodynamic applications with finite elasticity one really needs to solve exactly also the structure non-linearity, or if the latter can be linearized around a state suitably extrapolated from previous time steps. In particular, here we propose to solve at each time step a linearized elasticity problem, coupled with the fluid in a fixed domain, with both the structure linearization point and the fluid domain extrapolated from previous time steps. This approach would correspond to perform just one approximate-Newton iteration on the monolithic FSI problem, starting from a well-chosen initial guess. Alternatively, we propose to run just few Newton iterations at each time step, with the aim of improving the accuracy. We also consider the inexact variants of the fixed-point-based schemes, obtained by performing one or few external iterations, where again both the structure linearization point and the fluid domain are extrapolated from previous time steps.

The second goal of this work consists in studying the accuracy of such inexact schemes. When a globally third order accurate time discretization of the FSI problem is considered, we show numerically on a simple test case that performing at least two Newton iterations allows to recover a third order convergence in time even when starting from a first order extrapolation, while one Newton iteration is enough when starting form a third order extrapolation. We also show that such schemes are very accurate in the case of a real 3D case, and that they allow to improve the computational efficiency up to three times.

The outline of the work is as follows. In Section 2 we present the global FSI problem, its time discretization and a Lagrange multipliers formulation useful to derive the numerical schemes. In Section 3 we present the exact schemes. In particular, in Section 3.1 we introduce the classical partitioned algorithms, in Section 3.2 those based on the approximate-Newton method, and in Section 3.3 the new family based on a fixed-point reformulation of the global FSI problem. In Section 3.5 we study the efficiency of such schemes by considering a real case in haemodynamics. Then, in Section 4 we introduce the inexact schemes, both those derived by approximate-Newton-based methods (Section 4.1) and those derived by fixed-point-based methods (Section 4.2). Finally, in Section 4.3 we provide the convergence rates of inexact methods used to solve an analytical test case, and in Section 4.4 we provide a study on the accuracy and efficiency of such schemes applied to a real haemodynamic case.

2 The FSI problem and its time discretization

Referring to the fluid domain Ω_f^t like the one represented in Figure 1, left, we denote, for any function v living in the current fluid configuration, by $\widetilde{v} := v \circ \mathcal{A}$ its counterpart in the reference configuration Ω_f^0, where $\mathcal{A}$ is the ALE map. By considering instead the structure domain Ω_s^t like the one represented in Figure 1, right, we denote, for any function g defined in the current solid configuration, by $\widetilde{g} := g \circ \mathcal{L}$ its counterpart in the reference domain Ω_s^0, where $\mathcal{L}$ is the Lagrangian

map. The strong formulation of the FSI problem, including the computation of

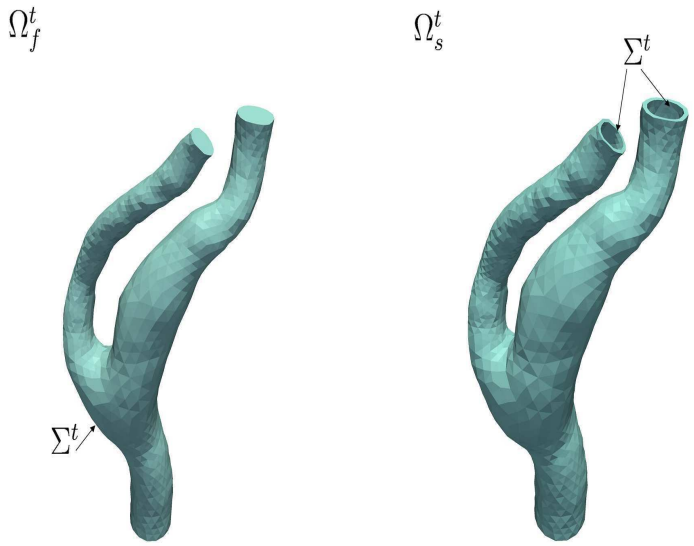

Figure 1: Representation of the domain of the FSI problem: fluid domain on the left, structure domain on the right.

the ALE map reads then as follows:

1. *Fluid-Structure problem.* Given the (unknown) fluid domain velocity $\boldsymbol{u}_m$ and fluid domain Ω_f^t, find, at each time $t \in (0, T]$, fluid velocity $\boldsymbol{u}_f$, pressure p_f and structure displacement $\boldsymbol{\eta}_s$ such that

$$\begin{cases} \rho_f \dfrac{D^A \boldsymbol{u}_f}{Dt} + \rho_f((\boldsymbol{u}_f - \boldsymbol{u}_m) \cdot \nabla)\boldsymbol{u}_f - \nabla \cdot \boldsymbol{T}_f(\boldsymbol{u}_f, p_f) = \boldsymbol{f}_f & \text{in } \Omega_f^t, \\ \nabla \cdot \boldsymbol{u}_f = 0 & \text{in } \Omega_f^t, \\ \boldsymbol{u}_f = \dfrac{\partial \boldsymbol{\eta}_s}{\partial t} & \text{on } \Sigma^t, \\ \boldsymbol{T}_s(\boldsymbol{\eta}_s)\,\boldsymbol{n} - \boldsymbol{T}_f(\boldsymbol{u}_f, p_f)\,\boldsymbol{n} = \boldsymbol{0} & \text{on } \Sigma^t, \\ \rho_s \dfrac{\partial^2 \widetilde{\boldsymbol{\eta}}_s}{\partial t^2} - \nabla \cdot \widetilde{\boldsymbol{T}}_s(\widetilde{\boldsymbol{\eta}}_s) = \widetilde{\boldsymbol{f}}_s & \text{in } \Omega_s^0, \end{cases} \tag{1}$$

   where ρ_f and ρ_s are the fluid and structure densities, μ is the constant blood viscosity, $\boldsymbol{f}_f$ and $\boldsymbol{f}_s$ the forcing terms, $\boldsymbol{n}$ the unit normal exiting from the structure domain, and $\frac{D^A}{Dt}$ denotes the ALE derivative;

2. *Geometry problem.* Given the (unknown) interface structure displacement $\widetilde{\boldsymbol{\eta}}_s|_{\Sigma^0}$, find the displacement of the points of the fluid domain $\boldsymbol{\eta}_m$ such that

$$\begin{cases} -\triangle \widetilde{\boldsymbol{\eta}}_m = \boldsymbol{0} & \text{on } \Omega_f^0, \\ \widetilde{\boldsymbol{\eta}}_m = \widetilde{\boldsymbol{\eta}}_s & \text{on } \Sigma^0, \end{cases} \tag{2}$$

and then find accordingly the fluid domain velocity $\widetilde{\boldsymbol{u}}_m := \frac{\partial \widetilde{\boldsymbol{\eta}}_m}{\partial t}$, the ALE map and the new points $\boldsymbol{x}_f^t$ of the fluid domain by moving the points $\boldsymbol{x}_f^0$ of the reference domain Ω_f^0:

$$\mathcal{A}(\boldsymbol{x}_f^0) = \boldsymbol{x}_f^t = \boldsymbol{x}_f^0 + \widetilde{\boldsymbol{\eta}}_m.$$

In the previous problem, $\boldsymbol{T}_f(\boldsymbol{u}_f, p_f)$ is the Cauchy stress tensor related to a homogeneous, Newtonian, incompressible fluid, whilst $\widetilde{\boldsymbol{T}}_s(\widetilde{\boldsymbol{\eta}}_s)$ and $\boldsymbol{T}_s(\boldsymbol{\eta}_s)$ are the first Piola-Kirchhoff and the Cauchy stress tensors of the solid, respectively, describing the structure problem. The two matching conditions enforced at the FS interface are the *continuity of velocities* $(1)_4$ and the *continuity of normal stresses* $(1)_5$ (physical interface conditions), whilst condition $(2)_2$ enforces the continuity at the FS interface of displacements of the fluid and structure subdomains (geometrical interface condition). Equations (1) and (2) have to be endowed with suitable boundary conditions on $\Omega_f^t \setminus \Sigma^t$ and $\Omega_s^0 \setminus \Sigma^0$, and with suitable initial conditions.

Let Δt be the time discretization parameter and $t^n := n\,\Delta t$, $n = 0, 1, \ldots$. For a generic function z, we denote with z^n the approximation of $z(t^n)$. We consider *Backward Differentiation Formulae* of order p (BDFp) of the form

$$\frac{D_p v^{n+1}}{\Delta t} := \frac{1}{\Delta t}\left(\beta_0\, v^{n+1} - \sum_{i=1}^{p} \beta_i\, v^{n+1-i}\right) = \frac{\partial v}{\partial t}(t^{n+1}) + O(\Delta t^p),$$
$$\frac{D_p^2 v^{n+1}}{\Delta t^2} := \frac{1}{\Delta t^2}\left(\xi_0\, v^{n+1} - \sum_{i=1}^{p+1} \xi_i\, v^{n+1-i}\right) = \frac{\partial^2 v}{\partial t^2}(t^{n+1}) + O(\Delta t^p),$$

for suitable coefficients β_i and ξ_i [38, 40]. We report here the formulation of the time discretization of order p of problem (1)-(2).

1. *Fluid-Structure problem.* Given the (unknown) fluid domain velocity $\boldsymbol{u}_m^{n+1}$ and the fluid domain Ω_f^{n+1} and the solution at previous time steps, find the fluid velocity $\boldsymbol{u}_f^{n+1}$, the pressure p_f^{n+1} and the structure displacement $\boldsymbol{\eta}_s^{n+1}$ such that

$$\begin{cases} \rho_f \dfrac{D_p\, \boldsymbol{u}_f^{n+1}}{\Delta t} + \rho_f((\boldsymbol{u}_f^{n+1} - \boldsymbol{u}_m^{n+1}) \cdot \nabla)\boldsymbol{u}_f^{n+1} - \nabla \cdot \boldsymbol{T}_f(\boldsymbol{u}_f^{n+1}, p_f^{n+1}) = \boldsymbol{f}_f^{n+1} & \text{in } \Omega_f^{n+1}, \\ \nabla \cdot \boldsymbol{u}_f^{n+1} = 0 & \text{in } \Omega_f^{n+1}, \\ \boldsymbol{u}_f^{n+1} = \boldsymbol{u}_s^{n+1} & \text{on } \Sigma^{n+1}, \\ \boldsymbol{T}_s(\boldsymbol{\eta}_s^{n+1})\,\boldsymbol{n} - \boldsymbol{T}_f(\boldsymbol{u}_f^{n+1}, p_f^{n+1})\,\boldsymbol{n} = \boldsymbol{0} & \text{on } \Sigma^{n+1}, \\ \rho_s \dfrac{D_p^2\, \widetilde{\boldsymbol{\eta}}_s^{n+1}}{\Delta t^2} - \nabla \cdot \widetilde{\boldsymbol{T}}_s(\widetilde{\boldsymbol{\eta}}_s^{n+1}) = \widetilde{\boldsymbol{f}}_s^{n+1} & \text{in } \Omega_s^0. \end{cases} \tag{3}$$

   In problem (3) we have also introduced the structure velocity $\boldsymbol{u}_s^n := \frac{D_p \boldsymbol{\eta}_s^n}{\Delta t}$.

2. *Geometry problem.* Given the (unknown) interface structure displacement $\widetilde{\boldsymbol{\eta}}_s^{n+1}|_{\Sigma^0}$, solve a harmonic extension problem

$$\begin{cases} -\triangle \widetilde{\boldsymbol{\eta}}_m^{n+1} = \mathbf{0} & \text{in } \Omega_f^0, \\ \widetilde{\boldsymbol{\eta}}_m^{n+1} = \widetilde{\boldsymbol{\eta}}_s^{n+1} & \text{on } \Sigma^0, \end{cases} \tag{4}$$

and then find accordingly the discrete fluid domain velocity $\widetilde{\boldsymbol{u}}_m^{n+1}$ and the points $\boldsymbol{x}_f^{n+1}$ of the new fluid domain by

$$\widetilde{\boldsymbol{u}}_m^{n+1} := \frac{D_p \widetilde{\boldsymbol{\eta}}_m^{n+1}}{\Delta t}, \qquad \boldsymbol{x}_f^{n+1} = \boldsymbol{x}_f^0 + \widetilde{\boldsymbol{\eta}}_m^{n+1}. \tag{5}$$

We consider here an equivalent formulation of (3) and (4) based on the introduction of three Lagrange multipliers living at the FS interface, representing the fluid and structure normal stresses $\boldsymbol{\lambda}_f$ and $\boldsymbol{\lambda}_s$, and the normal derivative of the fluid mesh displacement $\boldsymbol{\lambda}_m$ [38]. For the sake of notation we remove the temporal index $^{n+1}$. With Σ_f^D, $\Sigma_s^{D,0}$ and Σ_m^D we denote the parts of the boundary where Dirichlet boundary conditions are prescribed. Then, we define the following spaces

$$V_f := \{v \in H^1(\Omega_f) : v|_{\Sigma_f^D} = 0\}, \qquad Q := L^2(\Omega_f)^1,$$

$$V_s := \{v \in H^1(\Omega_s^0) : v|_{\Sigma_s^{D,0}} = 0\}, \qquad V_m := \{v \in H^1(\Omega_f^0) : v|_{\Sigma_m^{D,0}} = 0\}.$$

Let $\boldsymbol{v}_f := (\boldsymbol{u}_f, p_f)$ collect the fluid unknowns and $\mathcal{F} : \boldsymbol{V}_f \times Q \times \boldsymbol{V}_m \to (\boldsymbol{V}_f \times Q)'$ be the fluid operator. Analogously, for the structure subproblem we define the operator $\mathcal{S} : \boldsymbol{V}_s \to (\boldsymbol{V}_s)'$, and for the harmonic extension we introduce the operator $\mathcal{H} : \boldsymbol{V}_m \to (\boldsymbol{V}_m)'$. We then rewrite problem (3)-(4) as follows

$$\begin{cases} \mathcal{H}\,\widetilde{\boldsymbol{\eta}}_m + \widetilde{\gamma}_m^* \widetilde{\boldsymbol{\lambda}}_m &=& \mathbf{0} & \text{in } (\boldsymbol{V}_m)', \\ \widetilde{\gamma}_m \widetilde{\boldsymbol{\eta}}_m &=& \widetilde{\gamma}_s \widetilde{\boldsymbol{\eta}}_s & \text{on } \Sigma^0, \\ \mathcal{F}(\boldsymbol{v}_f, \boldsymbol{u}_m) + \widetilde{\gamma}_f^* \widetilde{\boldsymbol{\lambda}}_f &=& \mathcal{G}_f & \text{in } (\boldsymbol{V}_f \times Q)', \\ \alpha_f\, \widetilde{\gamma}_f \boldsymbol{v}_f + \widetilde{\boldsymbol{\lambda}}_f &=& \alpha_f \widetilde{\gamma}_s \frac{D_p \widetilde{\boldsymbol{\eta}}_s}{\Delta t} - \widetilde{\boldsymbol{\lambda}}_s & \text{on } \Sigma^0, \\ \alpha_s \widetilde{\gamma}_s \frac{D_p \widetilde{\boldsymbol{\eta}}_s}{\Delta t} + \widetilde{\boldsymbol{\lambda}}_s &=& \alpha_s \widetilde{\gamma}_f \boldsymbol{v}_f - \widetilde{\boldsymbol{\lambda}}_f & \text{on } \Sigma^0, \\ \mathcal{S}(\widetilde{\boldsymbol{\eta}}_s) + \widetilde{\gamma}_s^* \widetilde{\boldsymbol{\lambda}}_s &=& \mathcal{G}_s & \text{in } (\boldsymbol{V}_s)', \end{cases} \tag{6}$$

where $\widetilde{\gamma}_f : \boldsymbol{V}_f \times Q \to \boldsymbol{H}^{1/2}(\Sigma^0)$, $\widetilde{\gamma}_s : \boldsymbol{V}_s \to \boldsymbol{H}^{1/2}(\Sigma^0)$, $\widetilde{\gamma}_m : \boldsymbol{V}_m \to \boldsymbol{H}^{1/2}(\Sigma^0)$ are trace operators and $\widetilde{\gamma}_f^*$, $\widetilde{\gamma}_s^*$, $\widetilde{\gamma}_m^*$ are their adjoints, $\mathcal{G}_s$ and $\mathcal{G}_f$ account for the right hand sides, $(6)_2$ is the geometrical interface condition, and the interface physical conditions $(6)_{3-4}$ are linear combinations of conditions $(3)_{3-4}$ through coefficients α_f and α_s. This will allow to obtain partitioned algorithms based on Robin interface conditions, which have good convergence properties, independent of the added-mass effect when the parameters α_f and α_s are suitably chosen [3, 4, 1, 22].

[1] Since we solve the FSI problem in a partitioned way with Robin conditions at the FS interface (see (6)), the pressure is always defined and $L^2(\Omega_f)$ is the suitable pressure space for the weak formulation.

2.1 Outlook of iterative algorithms

As discussed above, we have to face three sources of coupling and non-linearities, namely

(G) the geometrical interface condition;

(C) the constitutive non-linearities;

(P) the physical interface conditions.

We give here an outlook of the partitioned algorithms considered in the following sections. In principle, our model algorithm will consist of three nested loops, one for each of the three sources of coupling and non-linearities summarized above. Just to fix the ideas, we suppose here that the external loop will manage the geometrical interface condition, the intermediate one the constitutive non-linearities and the internal one the physical interface conditions. Our model algorithm is then of the type

```
while (geometrical interface condition not satisfied) do
 ...
   while (constitutive non-linearities not satisfied) do
    ...
      while (physical interface conditions not satisfied) do
       ...
      end
   end
end
```

We call this algorithm G∞-C∞-P∞, where ∞ means that we let the iterations continue until convergence. Starting from this model scheme, we can obtain many other algorithms as follows.

1. The order of the loops could be exchanged, leading to different schemes (G∞-P∞-C∞, ...);

2. We can merge two or more loops. For example, starting from the model algorithm G∞-C∞-P∞, we could decide to treat in the same loop the geometrical interface condition and the constitutive non-linearities, obtaining the algorithm GC∞-P∞.

3. The external loop could be solved not until convergence, but performing just few external iterations. In this case, such algorithms have to be intended as *inexact*, since the external stopping criterion is not checked and satisfied. For example, starting from our model scheme, we could decide to do just 2 external iterations, obtaining the algorithm I-G2-C∞-P∞, where we put a letter I at the beginning to emphasize that such scheme is inexact.

4. In the case of inexact schemes where only few (even one) iterations are performed in the external loop, we could consider starting the iterations from an initial guess obtained by a $p-th$ order extrapolation in time. In this case, we add the letter E after the number of iterations of the loop involving the extrapolation. For example, starting from the model algorithm with just 1 external iterations, if we decided to use an extrapolation of the interface position as initial guess, we name the corresponding scheme as I-G1E-C∞-P∞. In this work, we have always used the same order p for the extrapolation as the order of the temporal scheme.

3 Exact schemes

We discuss here the family of exact schemes, that is schemes which satisfy exactly, up to given tolerances, the three interface conditions and the constitutive non-linearities. In particular, we describe the classical schemes, the approximate-Newton-based scheme and the new family of fixed-point-based scheme. Then, in Section 3.5, the performance of these schemes will be compared for the first time for a real haemodynamic case, by using an exponential law for the structure strain energy.

3.1 Classical scheme

The first strategy corresponds to simple iterations at each time step between the fluid geometry, the fluid and the structure subproblems (see [24, 29, 31, 27] for the Dirichlet-Neumann case). Here, we present the Robin-Robin version of such schemes introduced in [40]. In particular, we have the following

Algorithm 3.1 GP∞-C∞ scheme.

Given the solution at iteration k, solve until convergence

1. The fluid geometric problem

$$\left\{ \begin{array}{rcll} \mathcal{H}\,\widetilde{\boldsymbol{\eta}}_m^{k+1} + \widetilde{\gamma}_m^* \widetilde{\boldsymbol{\lambda}}_m^{k+1} & = & \mathbf{0} & \text{in } (\boldsymbol{V}_m)', \\ \widetilde{\gamma}_m \widetilde{\boldsymbol{\eta}}_m^{k+1} & = & \widetilde{\gamma}_s \widetilde{\boldsymbol{\eta}}_s^{k} & \text{on } \Sigma^0, \end{array} \right. \tag{7}$$

2. The (non-linear) fluid problem in ALE configuration with Robin interface condition

$$\left\{ \begin{array}{rcll} \mathcal{F}(\boldsymbol{v}_f^{k+1}, \boldsymbol{u}_m^{k+1}) + \widetilde{\gamma}_f^* \widetilde{\boldsymbol{\lambda}}_f^{k+1} & = & \mathcal{G}_f & \text{in } \left(\boldsymbol{V}_f(\boldsymbol{\eta}_m^{k+1}) \times Q(\boldsymbol{\eta}_m^{k+1})\right)', \\ \alpha_f\, \gamma_f \boldsymbol{v}_f^{k+1} + \boldsymbol{\lambda}_f^{k+1} & = & \alpha_f \gamma_s \frac{D_p \boldsymbol{\eta}_s^k}{\Delta t} - \boldsymbol{\lambda}_s^k & \text{on } \Sigma^{k+1}; \end{array} \right. \tag{8}$$

3. The (non-linear) structure problem with Robin interface condition

$$\left\{\begin{array}{rcll} \mathcal{S}(\widetilde{\boldsymbol{\eta}}_s^{k+1}) + \widetilde{\gamma}_s^* \widetilde{\boldsymbol{\lambda}}_s^{k+1} & = & \mathcal{G}_s & \text{in } (\boldsymbol{V}_s)', \\ \alpha_s \widetilde{\gamma}_s \frac{D_p \widetilde{\boldsymbol{\eta}}_s^{k+1}}{\Delta t} + \widetilde{\boldsymbol{\lambda}}_s^{k+1} & = & \alpha_s \widetilde{\gamma}_f \boldsymbol{v}_f^{k+1} - \widetilde{\boldsymbol{\lambda}}_f^{k+1} & \text{on } \Sigma^0; \end{array}\right.$$

4. Relaxation step

$$\widetilde{\boldsymbol{\eta}}_s^{k+1} = \omega\, \widetilde{\boldsymbol{\eta}}_s^{k+1} + (1-\omega)\widetilde{\boldsymbol{\eta}}_s^{k},$$

where $\omega \in (0, 1]$ is a relaxation parameter.

At step 2. we have highlighted the dependence of $\boldsymbol{V}_f$ and Q_f on $\boldsymbol{\eta}_m^{k+1}$. We monitor the residuals of conditions $(7)_2$ and $(8)_2$ and stop the iterations when such residuals are below a prescribed tolerance.

At each iteration of the previous algorithm, the fluid and structure subproblems have to be solved with a proper strategy to handle the non-linearities, such as with Picard iterations for the fluid and Newton iterations for the structure. Algorithm 3.1 has a double-loop nature and, according to the notation introduced in Section 2.1, it will denoted in what follows as GP∞-C∞.

3.2 Approximate-Newton-based schemes

We present here the prototype of such family of schemes, which combines an approximate-Newton scheme for the monolithic FSI problem with Robin-Robin subiterations for the linearized problem. This is given by the following

Algorithm 3.2 GC∞-P∞ scheme

[**External loop - index k**]. Given the solution at iteration k, solve until convergence

1. The harmonic extension

$$\left\{\begin{array}{rcll} \mathcal{H}\, \widetilde{\boldsymbol{\eta}}_m^{k+1} + \widetilde{\gamma}_m^* \widetilde{\boldsymbol{\lambda}}_m^{k+1} & = & 0 & \text{in } (\boldsymbol{V}_m)', \\ \widetilde{\gamma}_m \widetilde{\boldsymbol{\eta}}_m^{k+1} & = & \widetilde{\gamma}_s \widetilde{\boldsymbol{\eta}}_s^{k} & \text{on } \Sigma^0, \end{array}\right. \tag{9}$$

obtaining the new fluid domain and fluid domain velocity;

2. The linearized FSI problem. For its solution, we consider the following partitioned algorithm:

[**Internal loop - index l**] Given the solution at subiteration $l-1$, solve at current subiteration l until convergence

(a) The fluid subproblem with a Robin condition at the FS interface

$$\left\{\begin{array}{rcll} \widehat{\nabla}_{v_f} \mathcal{F}(\boldsymbol{u}_f^k - \boldsymbol{u}_m^{k+1})\, \boldsymbol{v}_{f,l}^{k+1} + \widetilde{\gamma}_f^* \widetilde{\boldsymbol{\lambda}}_{f,l}^{k+1} & = & \mathcal{G}_f & \text{in } \left(\boldsymbol{V}_f(\boldsymbol{\eta}_m^{k+1}) \times Q_f(\boldsymbol{\eta}_m^{k+1})\right)', \\ \alpha_f \gamma_f \boldsymbol{v}_{f,l}^{k+1} + \boldsymbol{\lambda}_{f,l}^{k+1} & = & \alpha_f \gamma_s \frac{D_p\, \boldsymbol{\eta}_{s,l-1}^{k+1}}{\Delta t} - \boldsymbol{\lambda}_{s,l-1}^{k+1} & \text{on } \Sigma^{k+1}; \end{array}\right. \tag{10}$$

(b) The structure subproblem with a Robin condition at the FS interface

$$\left\{\begin{array}{rcll} \nabla_\eta \mathcal{S}(\widetilde{\boldsymbol{\eta}}_s^k)\,\delta\widetilde{\boldsymbol{\eta}}_{s,l}^{k+1} + \widetilde{\gamma}_s^*\delta\widetilde{\boldsymbol{\lambda}}_{s,l}^{k+1} & = & \mathcal{G}_s - \mathcal{S}(\widetilde{\boldsymbol{\eta}}_s^k) - \widetilde{\gamma}_s^*\widetilde{\boldsymbol{\lambda}}_s^k & \text{in } (\boldsymbol{V}_s)', \\ \alpha_s\widetilde{\gamma}_s\dfrac{D_p\,\widetilde{\boldsymbol{\eta}}_{s,l}^{k+1}}{\Delta t} - \widetilde{\boldsymbol{\lambda}}_{s,l}^{k+1} & = & \alpha_s\widetilde{\gamma}_f\,\widetilde{\boldsymbol{v}}_{f,l}^{k+1} - \widetilde{\boldsymbol{\lambda}}_{f,l}^{k+1} & \text{on } \Sigma^0; \end{array}\right. \tag{11}$$

(c) Relaxation step

$$\widetilde{\boldsymbol{\eta}}_{s,l}^{k+1} = \omega\,\widetilde{\boldsymbol{\eta}}_{s,l}^{k+1} + (1-\omega)\widetilde{\boldsymbol{\eta}}_{s,l-1}^{k+1},$$

where $\widehat{\nabla}_{v_f}\mathcal{F}$ is the Oseen approximation of $\nabla_{v_f}\mathcal{F}$ with the convective term highlighted in the brackets. Such algorithm is obtained by applying the approximate-Newton method to the monolithic non-linear system (6), by considering as approximation of the Jacobian

$$\left[\begin{array}{cc|ccc|cc} \mathcal{H} & \widetilde{\gamma}_m^* & & & & & \\ \widetilde{\gamma}_m & & & & & \multicolumn{2}{c}{\widetilde{\gamma}_s^*} \\ \hline \nabla_{u_m}\mathcal{F} & & \nabla_{v_f}\mathcal{F} & \widetilde{\gamma}_f^* & & & \\ & & \alpha_f\widetilde{\gamma}_f & I & I & \multicolumn{2}{c}{-\alpha_f\frac{\beta_{s,0}}{\Delta t}\widetilde{\gamma}_s} \\ \hline & & -\alpha_s\widetilde{\gamma}_f & I & I & \multicolumn{2}{c}{\alpha_s\frac{\beta_{s,0}}{\Delta t}\widetilde{\gamma}_s} \\ & & & & \widetilde{\gamma}_s^* & \multicolumn{2}{c}{\nabla_{\eta_s}\mathcal{S}} \end{array}\right],$$

the following expression

$$\widehat{J}_{DL} = \left[\begin{array}{cc|ccc|cc} \mathcal{H} & \widetilde{\gamma}_m^* & & & & & \\ \widetilde{\gamma}_m & & & & & & \\ \hline & & \widehat{\nabla}_{v_f}\mathcal{F} & \widetilde{\gamma}_f^* & & & \\ & & \alpha_f\widetilde{\gamma}_f & I & I & \multicolumn{2}{c}{-\alpha_f\frac{\beta_{s,0}}{\Delta t}\widetilde{\gamma}_s} \\ \hline & & -\alpha_s\widetilde{\gamma}_f & I & I & \multicolumn{2}{c}{\alpha_s\frac{\beta_{s,0}}{\Delta t}\widetilde{\gamma}_s} \\ & & & & \widetilde{\gamma}_s^* & \multicolumn{2}{c}{\nabla_{\eta_s}\mathcal{S}} \end{array}\right],$$

which neglects the term $\nabla_{u_m}\mathcal{F}$ involving the shape derivatives and the term $\widetilde{\gamma}_s^*$ which couples the fluid geometry and the structure problems [38].

This algorithm has a double-loop nature as Algorithm 3.1, however in this case the physical interface conditions are managed in the internal loop (GC∞-P∞ scheme). For the external loop, we monitor the residual of equation $(9)_2$ and the residuals related to the convergence of the non-linear terms in the fluid and in the structure subproblems. For the internal loop, we monitor the residual of equation $(10)_2$. In any case, we stop the external and internal iterations when the related residuals are below a prescribed tolerance.

Another scheme of this family, obtained by considering a different approximation of the Jacobian, is the so-called Single-loop (GCP∞) scheme [23, 33, 30, 38], where all the non-linearities and interface conditions are treated in the same loop. Such algorithm is obtained by applying the approximate-Newton method to the

monolithic non-linear system (6), by considering the following approximate Jacobian

$$\widehat{J}_{SL} = \left[\begin{array}{cc|cc|cc} \mathcal{H} & \widetilde{\gamma}_m^* & & & & \\ \widetilde{\gamma}_m & & & & & \\ \hline & & \widehat{\nabla}_{v_f}\mathcal{F} & \widetilde{\gamma}_f^* & & \\ & & \alpha_f\widetilde{\gamma}_f & I & & \\ \hline & & -\alpha_s\widetilde{\gamma}_f & I & I & \alpha_s\frac{\beta_{s,0}}{\Delta t}\widetilde{\gamma}_s \\ & & & & \widetilde{\gamma}_s^* & \nabla_{\eta_s}\mathcal{S}. \end{array}\right].$$

Single-loop scheme is also obtained by Algorithm 3.2 by performing just 1 internal iteration, however monitoring the residual of equation $(10)_2$.

3.3 Fixed-point-based schemes

In this section we present new algorithms, firstly proposed in [42], to solve the coupled FSI problem.

3.3.1 The fixed-point problem

We start from the Lagrange multipliers formulation (6) and we rewrite it as a fixed-point problem over the interface position. To this aim, we introduce the variable

$$\widetilde{\boldsymbol{\xi}}_s := \widetilde{\gamma}_s\widetilde{\boldsymbol{\eta}}_s,$$

that represents the solid displacement at the FS interface. Moreover, we define the following operators:

- The harmonic extension operator

$$\mathcal{H}^\dagger : \boldsymbol{H}^{1/2}(\widetilde{\Sigma}) \to \widetilde{\boldsymbol{V}}_m \times \widetilde{\boldsymbol{V}}_m, \quad (\widetilde{\boldsymbol{\eta}}_m, \widetilde{\boldsymbol{u}}_m) = \mathcal{H}^\dagger\widetilde{\boldsymbol{\xi}}_s,$$

defined as follows

$$(\widetilde{\boldsymbol{\eta}}_m, \widetilde{\boldsymbol{u}}_m) = \mathcal{H}^\dagger\widetilde{\boldsymbol{\xi}}_s : \quad \left\{\begin{array}{rcll} \mathcal{H}\,\widetilde{\boldsymbol{\eta}}_m + \widetilde{\gamma}_m^*\widetilde{\boldsymbol{\lambda}}_m &=& \boldsymbol{0} & \text{in } (\widetilde{\boldsymbol{V}}_m)', \\ \widetilde{\gamma}_m\widetilde{\boldsymbol{\eta}}_m &=& \widetilde{\boldsymbol{\xi}}_s & \text{on } \widetilde{\Sigma}, \\ \widetilde{\boldsymbol{u}}_m &=& \dfrac{D_p\widetilde{\boldsymbol{\eta}}_m}{\Delta t} & \text{in } \widetilde{\Omega}_f; \end{array}\right.$$

- The operator that represents the interaction between the fluid and the solid problems in a known given fluid domain,

$$\mathcal{F}\mathcal{S}^\dagger : \boldsymbol{V}_m \times \boldsymbol{V}_m \to \widetilde{\boldsymbol{V}}_s, \quad \widetilde{\boldsymbol{\eta}}_s = \mathcal{F}\mathcal{S}^\dagger(\boldsymbol{\eta}_m, \boldsymbol{u}_m).$$

Given $\boldsymbol{\eta}_m$ and $\boldsymbol{u}_m$, this operator is defined as follows

$$\widetilde{\boldsymbol{\eta}}_s = \mathcal{F}\mathcal{S}^\dagger(\boldsymbol{\eta}_m, \boldsymbol{u}_m) : \quad \left\{\begin{array}{rcll} \mathcal{F}(\boldsymbol{v}_f, \boldsymbol{u}_m) + \widetilde{\gamma}_f^*\widetilde{\boldsymbol{\lambda}}_f &=& \mathcal{G}_f & \text{in } (\boldsymbol{V}_f(\boldsymbol{\eta}_m) \times Q_f(\boldsymbol{\eta}_m))', \\ \alpha_f\,\widetilde{\gamma}_f\widetilde{\boldsymbol{v}}_f + \widetilde{\boldsymbol{\lambda}}_f &=& \alpha_f\widetilde{\gamma}_s\frac{D_p\widetilde{\boldsymbol{\eta}}_s}{\Delta t} - \widetilde{\boldsymbol{\lambda}}_s & \text{on } \widetilde{\Sigma}, \\ \alpha_s\widetilde{\gamma}_s\frac{D_p\widetilde{\boldsymbol{\eta}}_s}{\Delta t} + \widetilde{\boldsymbol{\lambda}}_s &=& \alpha_s\widetilde{\gamma}_f\widetilde{\boldsymbol{v}}_f - \widetilde{\boldsymbol{\lambda}}_f & \text{on } \widetilde{\Sigma}, \\ \mathcal{S}(\widetilde{\boldsymbol{\eta}}_s) + \widetilde{\gamma}_s^*\widetilde{\boldsymbol{\lambda}}_s &=& \mathcal{G}_s & \text{in } (\widetilde{\boldsymbol{V}}_s)'. \end{array}\right.$$

We can now introduce a map $\boldsymbol{\phi} : \boldsymbol{H}^{1/2}(\widetilde{\Sigma}) \rightarrow \boldsymbol{H}^{1/2}(\widetilde{\Sigma})$, defined as

$$\boldsymbol{\phi} := \widetilde{\gamma}_s \mathcal{F}\mathcal{S}^\dagger(\mathcal{H}^\dagger(\widetilde{\boldsymbol{\xi}}_s)), \qquad \widetilde{\boldsymbol{\xi}}_s \underbrace{\xrightarrow{\mathcal{H}^\dagger} (\widetilde{\boldsymbol{\eta}}_m, \widetilde{\boldsymbol{u}}_m) \xrightarrow{\mathcal{F}\mathcal{S}^\dagger} \widetilde{\boldsymbol{\eta}}_s \xrightarrow{\widetilde{\gamma}_s}}_{\boldsymbol{\phi}} \widetilde{\boldsymbol{\xi}}_s,$$

and then write problem (6) as a fixed-point problem: Find $\widetilde{\boldsymbol{\xi}}_s$ such that

$$\widetilde{\boldsymbol{\xi}}_s = \boldsymbol{\phi}(\widetilde{\boldsymbol{\xi}}_s). \tag{12}$$

3.3.2 The numerical algorithms

Problem (12) can be solved with a fixed-point iteration method:

$$\text{Given} \quad \widetilde{\boldsymbol{\xi}}_s^0, \quad \widetilde{\boldsymbol{\xi}}_s^{k+1} = \boldsymbol{\phi}(\widetilde{\boldsymbol{\xi}}_s^k), \quad k \geq 0. \tag{13}$$

This iterative algorithm written in extended form reads as follows:
Given the solution $\widetilde{\boldsymbol{\xi}}_s^k$ at iteration k, solve at the current iteration $k+1$ until convergence

1. *The fluid geometric problem*

$$\begin{cases} \mathcal{H}\,\widetilde{\boldsymbol{\eta}}_m^{k+1} + \widetilde{\gamma}_m^* \widetilde{\boldsymbol{\lambda}}_m^{k+1} &= \boldsymbol{0} \quad \text{in } (\widetilde{\boldsymbol{V}}_m)', \\ \widetilde{\gamma}_m \widetilde{\boldsymbol{\eta}}_m^{k+1} &= \widetilde{\boldsymbol{\xi}}_s^k \quad \text{on } \widetilde{\Sigma}, \end{cases}$$

   obtaining the new fluid domain and fluid domain velocity;

2. *The non-linear FSI problem defined in a known fluid domain*

$$\begin{cases} \mathcal{F}(\boldsymbol{v}_f^{k+1}, \boldsymbol{u}_m^{k+1}) + \widetilde{\gamma}_f^* \widetilde{\boldsymbol{\lambda}}_f &= \mathcal{G}_f & \text{in } (\boldsymbol{V}_f(\boldsymbol{\eta}_m^{k+1}) \times Q_f(\boldsymbol{\eta}_m^{k+1}))', \\ \alpha_f \widetilde{\gamma}_f \widetilde{\boldsymbol{v}}_f^{k+1} + \widetilde{\boldsymbol{\lambda}}_f^{k+1} &= \alpha_f \widetilde{\gamma}_s \frac{D_p \widetilde{\boldsymbol{\eta}}_s^{k+1}}{\Delta t} - \widetilde{\boldsymbol{\lambda}}_s^{k+1} & \text{on } \widetilde{\Sigma}, \\ \alpha_s \widetilde{\gamma}_s \frac{D_p \widetilde{\boldsymbol{\eta}}_s^{k+1}}{\Delta t} + \widetilde{\boldsymbol{\lambda}}_s^{k+1} &= \alpha_s \widetilde{\gamma}_f \widetilde{\boldsymbol{v}}_f^{k+1} - \widetilde{\boldsymbol{\lambda}}_f^{k+1} & \text{on } \widetilde{\Sigma}, \\ \mathcal{S}(\widetilde{\boldsymbol{\eta}}_s^{k+1}) + \widetilde{\gamma}_s^* \widetilde{\boldsymbol{\lambda}}_s^{k+1} &= \mathcal{G}_s & \text{in } (\widetilde{\boldsymbol{V}}_s)'; \end{cases} \tag{14}$$

3. *The solid displacement is then restricted to the interface $\widetilde{\Sigma}$ and updated, in case, with a relaxation step*

$$\widetilde{\boldsymbol{\xi}}_s^{k+1} = \omega_G \widetilde{\gamma}_s \widetilde{\boldsymbol{\eta}}_s^{k+1} + (1 - \omega_G) \widetilde{\boldsymbol{\xi}}_s^k,$$

   where $\omega_G \in (0, 1]$ is a relaxation parameter.

□

The second step of the previous algorithm (problem (14)) is a coupled FSI problem solved in a known fluid domain (obtained thanks to $\boldsymbol{\eta}_m^{k+1}$), but where

the constitutive non-linearities are still present. Therefore, to solve this problem we have to manage in an internal loop both such non-linearities and the physical interface conditions. To do this, we consider an approximate-Newton method. Different approximate Jacobians lead to different algorithms, which are presented in what follows.

1. Using a single internal loop - G∞-CP∞ scheme. In this case, we apply the approximate-Newton method to system (14), with the following approximation of the Jacobian

$$\widehat{P}_1 = \left[\begin{array}{cc|cc} \widehat{\nabla}_{v_f}\mathcal{F} & \widetilde{\gamma}_f^* & & \\ \alpha_f\widetilde{\gamma}_f & I & & \\ \hline -\alpha_s\widetilde{\gamma}_f & I & I & \alpha_s\frac{\beta_{s,0}}{\Delta t}\widetilde{\gamma}_s \\ & & \widetilde{\gamma}_s^* & \nabla_{\eta_s}\mathcal{S} \end{array}\right]. \tag{15}$$

This scheme then reads as follows

Algorithm 3.3 G∞-CP∞ scheme

[External loop - index k]. Given the solution $\widetilde{\boldsymbol{\xi}}_s^k$ at iteration k, solve at the current iteration $k+1$ until convergence

1. The fluid geometric problem

$$\left\{\begin{array}{rcll} \mathcal{H}\,\widetilde{\boldsymbol{\eta}}_m^{k+1} + \widetilde{\gamma}_m^*\widetilde{\boldsymbol{\lambda}}_m^{k+1} &=& \mathbf{0} & \text{in } (\widetilde{\boldsymbol{V}}_m)', \\ \widetilde{\gamma}_m\widetilde{\boldsymbol{\eta}}_m^{k+1} &=& \widetilde{\boldsymbol{\xi}}_s^k & \text{on } \widetilde{\Sigma}; \end{array}\right. \tag{16}$$

   obtaining the new fluid domain and fluid domain velocity.

2. The FSI problem in a known given fluid problem. For its solutions, we consider the following approximate-Newton-based partitioned algorithm:

   [Internal loop - index j] Given the solution at subiteration $j-1$, solve at the current subiteration j until convergence

   (a) The fluid subproblem with a Robin condition at the FS interface

$$\left\{\begin{array}{rcll} \widehat{\nabla}_{v_f}\mathcal{F}(\boldsymbol{u}_f^{k+1,j-1} - \boldsymbol{u}_m^{k+1})\,\boldsymbol{v}_f^{k+1,j} + \widetilde{\gamma}_f^*\widetilde{\boldsymbol{\lambda}}_f^{k+1,j} &=& \mathcal{G}_f & \text{in } (\boldsymbol{V}_f(\boldsymbol{\eta}_m^{k+1}) \times Q_f(\boldsymbol{\eta}_m^{k+1}))', \\ \alpha_f\gamma_f\boldsymbol{v}_f^{k+1,j} + \boldsymbol{\lambda}_f^{k+1,j} &=& \alpha_f\gamma_s\frac{D_p\,\boldsymbol{\eta}_s^{k+1,j-1}}{\Delta t} - \boldsymbol{\lambda}_s^{k+1,j-1} & \text{on } \Sigma^{k+1}, \end{array}\right. \tag{17}$$

   (b) The structure subproblem with a Robin condition at the FS interface

$$\left\{\begin{array}{rcll} \nabla_{\eta_s}\mathcal{S}(\widetilde{\boldsymbol{\eta}}_s^{k+1,j-1})\,\delta\widetilde{\boldsymbol{\eta}}_s^{k+1,j} + \widetilde{\gamma}_s^*\delta\widetilde{\boldsymbol{\lambda}}_s^{k+1,j} &=& \mathcal{G}_s - \mathcal{S}(\widetilde{\boldsymbol{\eta}}_s^{k+1,j-1}) - \widetilde{\gamma}_s^*\widetilde{\boldsymbol{\lambda}}_s^{k+1,j-1} & \text{in } (\widetilde{\boldsymbol{V}}_s)', \\ \alpha_s\widetilde{\gamma}_s\dfrac{D_p\,\widetilde{\boldsymbol{\eta}}_s^{k+1,j}}{\Delta t} - \widetilde{\boldsymbol{\lambda}}_s^{k+1,j} &=& \alpha_s\widetilde{\gamma}_f\,\widetilde{\boldsymbol{v}}_f^{k+1,j} - \widetilde{\boldsymbol{\lambda}}_f^{k+1,j} & \text{on } \widetilde{\Sigma}. \end{array}\right.$$

(c) Relaxation step

$$\widetilde{\boldsymbol{\eta}}_s^{k+1,j} = \omega_P \, \widetilde{\boldsymbol{\eta}}_s^{k+1,j} + (1-\omega_P)\widetilde{\boldsymbol{\eta}}_s^{k+1,j-1},$$

where $\omega_P \in (0,1]$ is a relaxation parameter.

3. The solid displacement is then restricted to the interface $\widetilde{\Sigma}$

$$\widetilde{\boldsymbol{\xi}}_s^{k+1} = \omega_G \, \widetilde{\gamma}_s \widetilde{\boldsymbol{\eta}}_s^{k+1} + (1-\omega_G)\widetilde{\boldsymbol{\xi}}_s^{k},$$

where $\omega_G \in (0,1]$ is a relaxation parameter.

□

To stop the external iterations, we monitor the residual of condition $(16)_2$, while to stop the internal iterations we monitor the residual of condition $(17)_2$ and the residuals related to the convergence of the non-linear terms in the fluid and in the structure subproblems.

Remark 3.1 *G∞-CP∞ algorithm has a double loop structure, as GC∞-P∞ described in Algorithm 3.2. The difference with that algorithm consists in the fact that there the structure Jacobian was updated just at each external iteration, while here it is updated at each internal iteration.*

2. Using two nested internal loops - G∞-C∞-P∞ scheme. In this case, we consider two nested loops to solve the FSI problem (14): an intermediate one to manage the constitutive non-linearities and an internal one to prescribe the physical interface conditions. This corresponds to use

$$\widehat{P}_2 = \left[\begin{array}{cc|cc} \widehat{\nabla}_{v_f}\mathcal{F} & \widetilde{\gamma}_f^* & & \\ \alpha_f\widetilde{\gamma}_f & I & I & -\alpha_f \frac{\beta_{s,0}}{\Delta t}\,\widetilde{\gamma}_s \\ \hline -\alpha_s\widetilde{\gamma}_f & I & I & \alpha_s \frac{\beta_{s,0}}{\Delta t}\,\widetilde{\gamma}_s \\ & & \widetilde{\gamma}_s^* & \nabla_{\eta_s}\mathcal{S} \end{array}\right],$$

as approximate Jacobian for the approximate-Newton method applied to problem (14). At each approximate-Newton iterations, we have a fully linearized FSI problem. This can be solved with a block-Gauss-Seidel preconditioner which has formally the same expression of (15), but where the structure Jacobian is built differently, as it will be clear by Remark 3.2. We have then the following

Algorithm 3.4 G∞-C∞-P∞ scheme

[External loop - index k]. Given the solution $\widetilde{\boldsymbol{\xi}}_s^k$ at iteration k, solve at the current iteration $k+1$ until convergence

1. The fluid geometric problem

$$\left\{\begin{array}{rcll} \mathcal{H}\,\widetilde{\boldsymbol{\eta}}_m^{k+1} + \widetilde{\gamma}_m^* \widetilde{\boldsymbol{\lambda}}_m^{k+1} & = & \mathbf{0} & \text{in } (\widetilde{\boldsymbol{V}}_m)', \\ \widetilde{\gamma}_m \widetilde{\boldsymbol{\eta}}_m^{k+1} & = & \widetilde{\boldsymbol{\xi}}_s^k & \text{on } \widetilde{\Sigma}; \end{array}\right. \tag{18}$$

obtaining the new fluid domain and fluid domain velocity.

2. The FSI problem in a known given domain. For its linearization, we consider the following approximate-Newton iterations:

[Intermediate loop - index j] Given the solution at subiteration $j-1$, solve at the current subiteration j until convergence

$$\left\{\begin{array}{ll} \widehat{\nabla}_{v_f}\mathcal{F}(\boldsymbol{u}_f^{k+1,j-1} - \boldsymbol{u}_m^{k+1})\,\boldsymbol{v}_f^{k+1,j} + \widetilde{\gamma}_f^* \widetilde{\boldsymbol{\lambda}}_f^{k+1,j} = \mathcal{G}_f & \text{in } (\boldsymbol{V}_f(\widetilde{\boldsymbol{\eta}}_m^{k+1}) \times Q_f(\widetilde{\boldsymbol{\eta}}_m^{k+1}))', \\ \alpha_f\gamma_f \boldsymbol{v}_f^{k+1,j} + \boldsymbol{\lambda}_f^{k+1,j} = \alpha_f\gamma_s \frac{D_p\,\boldsymbol{\eta}_s^{k+1,j}}{\Delta t} - \boldsymbol{\lambda}_s^{k+1,j} & \text{on } \Sigma^{k+1}, \\ \alpha_s\widetilde{\gamma}_s \dfrac{D_p\,\widetilde{\boldsymbol{\eta}}_s^{k+1,j}}{\Delta t} - \widetilde{\boldsymbol{\lambda}}_s^{k+1,j} = \alpha_s\widetilde{\gamma}_f\,\widetilde{\boldsymbol{v}}_f^{k+1,j} - \widetilde{\boldsymbol{\lambda}}_f^{k+1,j} & \text{on } \widetilde{\Sigma}, \\ \nabla_{\eta_s}\mathcal{S}(\widetilde{\boldsymbol{\eta}}_s^{k+1,j-1})\,\delta\widetilde{\boldsymbol{\eta}}_s^{k+1,j} + \widetilde{\gamma}_s^*\delta\widetilde{\boldsymbol{\lambda}}_s^{k+1,j} = & \\ \qquad \mathcal{G}_s - \mathcal{S}(\widetilde{\boldsymbol{\eta}}_s^{k+1,j-1}) - \widetilde{\gamma}_s^*\widetilde{\boldsymbol{\lambda}}_s^{k+1,j-1} & \text{in } (\widetilde{\boldsymbol{V}}_s)'. \end{array}\right. \tag{19}$$

At each iteration of the intermediate loop this problem is still coupled through the physical interface conditions. For this reason we consider a Robin-Robin partitioned algorithm for its solution:

[Internal loop - index l] Given the solution at subiteration $l-1$, solve at the current subiteration l until convergence

(a) The fluid subproblem with a Robin condition at the FS interface

$$\left\{\begin{array}{l} \widehat{\nabla}_{v_f}\mathcal{F}(\boldsymbol{u}_f^{k+1,j-1} - \boldsymbol{u}_m^{k+1})\,\boldsymbol{v}_{f,l}^{k+1,j} + \widetilde{\gamma}_f^*\widetilde{\boldsymbol{\lambda}}_{f,l}^{k+1,j} = \mathcal{G}_f \quad \text{in } \left(\boldsymbol{V}_f(\widetilde{\boldsymbol{\eta}}_m^{k+1}) \times Q_f(\widetilde{\boldsymbol{\eta}}_m^{k+1})\right)', \\ \alpha_f\gamma_f\boldsymbol{v}_{f,l}^{k+1,j} + \boldsymbol{\lambda}_{f,l}^{k+1,j} = \alpha_f\gamma_s\frac{D_p\,\boldsymbol{\eta}_{s,l-1}^{k+1,j}}{\Delta t} - \boldsymbol{\lambda}_{s,l-1}^{k+1,j} \quad \text{on } \Sigma^{k+1}, \end{array}\right.$$

(b) The structure subproblem with a Robin condition at the FS interface

$$\left\{\begin{array}{ll} \nabla_{\eta_s}\mathcal{S}(\widetilde{\boldsymbol{\eta}}_s^{k+1,j-1})\,\delta\widetilde{\boldsymbol{\eta}}_{s,l}^{k+1,j} + \widetilde{\gamma}_s^*\delta\widetilde{\boldsymbol{\lambda}}_{s,l}^{k+1,j} = \mathcal{G}_s - \mathcal{S}(\widetilde{\boldsymbol{\eta}}_s^{k+1,j-1}) - \widetilde{\gamma}_s^*\widetilde{\boldsymbol{\lambda}}_s^{k+1,j-1} & \text{in } (\widetilde{\boldsymbol{V}}_s)', \\ \alpha_s\widetilde{\gamma}_s\,\dfrac{D_p\,\widetilde{\boldsymbol{\eta}}_{s,l}^{k+1,j}}{\Delta t} - \widetilde{\boldsymbol{\lambda}}_{s,l}^{k+1,j} = \alpha_s\widetilde{\gamma}_f\,\widetilde{\boldsymbol{v}}_{f,l}^{k+1,j} - \widetilde{\boldsymbol{\lambda}}_{f,l}^{k+1,j} & \text{on } \widetilde{\Sigma}. \end{array}\right.$$

(c) Relaxation step

$$\widetilde{\boldsymbol{\eta}}_{s,l}^{k+1,j} = \omega_P\,\widetilde{\boldsymbol{\eta}}_{s,l}^{k+1,j} + (1-\omega_P)\widetilde{\boldsymbol{\eta}}_{s,l-1}^{k+1,j},$$

where $\omega_P \in (0,1]$ is a relaxation parameter.

3. The solid displacement is then restricted to the interface $\widetilde{\Sigma}$

$$\widetilde{\boldsymbol{\xi}}_s^{k+1} = \omega_G \, \widetilde{\gamma}_s \widetilde{\boldsymbol{\eta}}_s^{k+1} + (1 - \omega_G) \widetilde{\boldsymbol{\xi}}_s^{k}, \tag{20}$$

where $\omega_G \in (0, 1]$ is a relaxation parameter.

□

To stop the external iterations, we monitor the residual of condition $(18)_2$. Regarding the intermediate iterations, we monitor the residuals related to the convergence of the non-linear terms in the fluid and in the structure subproblems. Finally, to stop the internal iterations we monitor the residual of condition $(19)_2$.

Remark 3.2 *G∞-C∞-P∞ algorithm has a triple loop nature. We observe that the structure Jacobian is updated at each intermediate iteration, by evaluating it for a structure displacement* $(\widetilde{\boldsymbol{\eta}}_s^{k+1,j-1})$ *which satisfies exactly the physical interface conditions, differently from that used to update the structure Jacobian in G∞-CP∞ algorithm, which does not satisfy them.*

3. Using two nested internal loops - G∞-P∞-C∞ scheme. This scheme is obtained by exchanging the order of the loops in G∞-C∞-P∞ scheme, that is by treating the constitutive non-linearities in the internal one. Even if we presented such algorithm as a fixed-point-based scheme, in the numerical results we will consider it as a classical one, due to its implementation based on solving in an iterative framework the non-linear fluid and structure subproblems. For the sake of brevity, we do not report here the detailed description of this algorithm.

3.4 An efficient choice of the internal tolerance

In the algorithms presented in previous sections, whenever Newton or approximate-Newton iterations are considered, the linear systems involved at each iteration do not need to be solved until convergence when an iterative method is considered. Indeed, as observed for example in [28], it is enough to stop the internal iterations when the residual is below a tolerance which is proportional to the Newton residual. This leads to a great saving in the computational times, without affecting the accuracy, since at convergence of the Newton iterations the tolerance of the internal linear system has become sufficiently low.

It is then possible to apply such idea to our cases, in particular to GC∞-P∞ and G∞-C∞-P∞. In both cases, the FSI linear system arising at each Newton iteration (step 2. in Algorithm 3.2 and step b. in Algorithm 3.4, respectively) does not need to be solved until convergence. This means that the physical interface conditions are in fact not satisfied at each approximate-Newton iteration. However, at convergence of the approximate-Newton loop, they are satisfied, so that these schemes are in fact exact.

In [28] such strategy is referred to as *inexact-Newton*. However, in order to avoid confusion with the inexact schemes presented in Section 4, we name these

algorithms *exact schemes with dynamic tolerance* and we add the suffix DT at the end of the name. In what follows, we detail GC∞-P∞-DT scheme.

Algorithm 3.5 GC∞-P∞-DT scheme

[**External loop - index k**]. Given the solution at iteration k, solve until convergence

1. The harmonic extension

$$\left\{\begin{array}{rcll} \mathcal{H}\,\widetilde{\boldsymbol{\eta}}_m^{k+1} + \widetilde{\gamma}_m^*\widetilde{\boldsymbol{\lambda}}_m^{k+1} &=& 0 & \text{in } (\boldsymbol{V}_m)', \\ \widetilde{\gamma}_m\widetilde{\boldsymbol{\eta}}_m^{k+1} &=& \widetilde{\gamma}_s\widetilde{\boldsymbol{\eta}}_s^{k} & \text{on } \Sigma^0, \end{array}\right. \tag{21}$$

   obtaining the new fluid domain and fluid domain velocity;

2. The linearized FSI problem. For its solution, given the external residual

$$\mathcal{R}^{k+1} := \|\widetilde{\gamma}_s\,\widetilde{\boldsymbol{\eta}}_s^{k+1} - \widetilde{\gamma}_s\,\widetilde{\boldsymbol{\eta}}_s^{k}\|_X + \|((\boldsymbol{u}_f^{k+1} - \boldsymbol{u}_f^{k})\cdot\nabla)\,\boldsymbol{u}_f^{k+1}\|_W + \|\mathcal{G}_s - \mathcal{S}(\widetilde{\boldsymbol{\eta}}_s^{k+1}) - \widetilde{\gamma}_s^*\widetilde{\boldsymbol{\lambda}}_s^{k+1}\|_K,$$

   we consider the following partitioned algorithm:

   [**Internal loop - index l**] Given the solution at subiteration $l-1$ and a suitable scalar σ^{k+1}, solve at current subiteration l until

$$\left\| \frac{\alpha_f\beta_0}{\Delta t}\left(\widetilde{\gamma}_s\widetilde{\boldsymbol{\eta}}_{s,l}^{k+1} - \widetilde{\gamma}_s\,\widetilde{\boldsymbol{\eta}}_{s,l-1}^{k+1}\right) + \widetilde{\boldsymbol{\lambda}}_{s,l}^{k+1} - \widetilde{\boldsymbol{\lambda}}_{s,l-1}^{k+1} \right\|_Z \leq \sigma^{k+1}\mathcal{R}^{k+1},$$

   (a) The fluid subproblem with a Robin condition at the FS interface

$$\left\{\begin{array}{rcl} \widehat{\nabla}_{v_f}\mathcal{F}(\boldsymbol{u}_{f,l}^{k} - \boldsymbol{u}_m^{k+1})\,\boldsymbol{v}_{f,l}^{k+1} + \widetilde{\gamma}_f^*\widetilde{\boldsymbol{\lambda}}_{f,l}^{k+1} &=& \mathcal{G}_f \quad \text{in } \left(\boldsymbol{V}_f(\boldsymbol{\eta}_m^{k+1})\times Q_f(\boldsymbol{\eta}_m^{k+1})\right)', \\ \alpha_f\gamma_f\boldsymbol{v}_{f,l}^{k+1} + \boldsymbol{\lambda}_{f,l}^{k+1} &=& \alpha_f\gamma_s\frac{D_p\,\boldsymbol{\eta}_{s,l-1}^{k}}{\Delta t} - \boldsymbol{\lambda}_{s,l-1}^{k} \quad \text{on } \Sigma^{k+1}; \end{array}\right. \tag{22}$$

   (b) The structure subproblem with a Robin condition at the FS interface

$$\left\{\begin{array}{rcll} \nabla_\eta\mathcal{S}(\widetilde{\boldsymbol{\eta}}_{s,l}^{k})\,\delta\widetilde{\boldsymbol{\eta}}_{s,l}^{k+1} + \widetilde{\gamma}_s^*\delta\widetilde{\boldsymbol{\lambda}}_{s,l}^{k+1} &=& \mathcal{G}_s - \mathcal{S}(\widetilde{\boldsymbol{\eta}}_s^{k}) - \widetilde{\gamma}_s^*\widetilde{\boldsymbol{\lambda}}_s^{k} & \text{in } (\boldsymbol{V}_s)', \\ \alpha_s\widetilde{\gamma}_s\dfrac{D_p\,\widetilde{\boldsymbol{\eta}}_{s,l}^{k+1}}{\Delta t} - \widetilde{\boldsymbol{\lambda}}_{s,l}^{k+1} &=& \alpha_s\widetilde{\gamma}_f\,\widetilde{\boldsymbol{v}}_{f,l}^{k+1} - \widetilde{\boldsymbol{\lambda}}_{f,l}^{k+1} & \text{on } \Sigma^0; \end{array}\right. \tag{23}$$

   (c) Relaxation step

$$\widetilde{\boldsymbol{\eta}}_{s,l}^{k+1} = \omega\,\widetilde{\boldsymbol{\eta}}_{s,l}^{k+1} + (1-\omega)\widetilde{\boldsymbol{\eta}}_{s,l-1}^{k+1}.$$

For the choice of σ^k we follow [28]. In particular, we set

$$\sigma^k = \begin{cases} \sigma_{max} & k = 0, \\ \min\left(\sigma_{max}, \gamma\left(\mathcal{R}^k/\mathcal{R}^{k-1}\right)^2\right) & k > 0,\ \gamma(\sigma^{k-1})^2 \leq 0.1, \\ \min\left(\sigma_{max}, \max\left(\gamma\left(\mathcal{R}^k/\mathcal{R}^{k-1}\right)^2, \gamma(\sigma^{k-1})^2\right)\right) & k > 0,\ \gamma(\sigma^{k-1})^2 > 0.1. \end{cases} \tag{24}$$

In the numerical simulations presented in this work we have used $\sigma_{max} = 0.9999$ and $\gamma = 0.9$. In the computation of the residuals, X, W, Z, K are suitable Sobolev spaces. In particular, the right choice is $X = H^{1/2}(\Sigma^0)$, $W = H^{-1}(\Omega_f)$, $Z = H^{-1/2}(\Sigma^0)$, $K = H^{-1}(\Omega_s)$. However, due to the complexity in the computation of these norms, in practical implementations we considered $W = L^2(\Omega_f)$, $K = L^2(\Omega_s)$ and $X = Z = L^2(\Sigma^0)$.

Remark 3.3 *In [28] it has been shown that the choice* (24) *guarantees a second order convergence when the exact Newton is considered. For approximate-Newton strategies, as in our case, this choice allows to recover first order of convergence.*

3.5 Numerical results for exact schemes

3.5.1 Generalities

In all the numerical experiments of this work, we considered the nearly incompressible *exponential* material whose first Piola-Kirchhoff tensor reads

$$\widetilde{\boldsymbol{T}}_s(\boldsymbol{F}_s) = GJ_s^{-2/3}\left(\boldsymbol{F}_s - \frac{1}{3}\mathrm{tr}(\boldsymbol{F}_s^T\boldsymbol{F}_s)\boldsymbol{F}_s^{-\mathrm{T}}\right)e^{\gamma(J_s^{-\frac{2}{3}}\mathrm{tr}(\boldsymbol{F}_s^T\boldsymbol{F}_s)-3)} + \frac{\kappa}{2}\left(J_s - 1 + \frac{1}{J_s}\ln(J_s)\right)J_s\boldsymbol{F}_s^{-\mathrm{T}}, \tag{25}$$

whose related energy is given by

$$W(\boldsymbol{F}_s) = \frac{G}{2\gamma}\left(e^{\gamma(J_s^{-\frac{2}{3}}\mathrm{tr}(\boldsymbol{F}_s^T\boldsymbol{F}_s)-3)} - 1\right) + \frac{\kappa}{4}\left((J_s-1)^2 + (\ln J_s)^2\right).$$

Here $\boldsymbol{F}_s := \nabla_{\boldsymbol{x}_s^0}\boldsymbol{x}_s^t$, with $\boldsymbol{x}_s^0$ the coordinates in the reference configuration and $\boldsymbol{x}_s^t$ those in the current configuration, $J_s := det(\boldsymbol{F}_s)$, κ is the *bulk modulus* and G the *shear modulus*. For small deformations such material behaves as a linear structure described by the infinitesimal elasticity, characterized by a Poisson's ratio ν and a Young modulus E related to κ and G as follows

$$\kappa = \frac{E}{3(1-2\nu)}, \qquad G = \frac{E}{2(1+\nu)}.$$

The parameter γ characterizes the stiffness of the material for large displacements.

Moreover, we used $P1bubble - P1$ finite elements for the fluid subproblem and $P1$ finite elements for the structure subproblem, and the following data: final time $T = 0.4\,s$, viscosity $\mu = 0.03\,g/(cm\,s)$, fluid density $\rho_f = 1\,g/cm^3$, structure density $\rho_s = 1.2\,g/cm^3$, bulk modulus $\kappa = 10^7\,dyne/cm^2$, shear modulus $G =$

$1.034 \cdot 10^6\, dyne/cm^2$ (corresponding for small displacements to Young modulus $E = 3 \cdot 10^6\, dyne/cm^2$ and Poisson ratio $\nu = 0.45$), $\gamma = 1$. Moreover, if not otherwise specified, we used as time discretization parameter $\Delta t = 0.002\, s$.

For the prescription of the interface continuity conditions, in all the simulations we have considered the Robin-Robin (RR) scheme [3, 4], with the optimized coefficients proposed in [22] and adapted to the various temporal schemes in [38]. To compute the optimal α_f we have used the value of $E = 3 \cdot 10^6\, dyne/cm^2$. In all the simulations of this work, RR scheme has converged without any relaxation, confirming its suitability for haemodynamic applications.

The numerical experiments have been performed with the parallel Finite Element library `LIFEV` (`www.lifev.org`), see [38] for details.

3.5.2 Efficiency of exact schemes in a real test case

In all the simulations of this section and of Section 4.4 we considered the computational domain depicted in Figure 1, representing the real carotid of a patient, after the removal of a plaque. The vessel lumen has been reconstructed by using the code VMTK (see `www.vmtk.org`), while the structure geometry has been obtained by extrusion, by setting the ratio between the lumen radius and the thickness equal to 0.24. The number of degrees of freedom is 160000 for the fluid domain and 30000 for the structure, and the fluid and structure meshes are conforming at the interface. For the harmonic extension and for the structure, we prescribed at the artificial sections normal homogeneous Dirichlet conditions and tangential homogeneous Neumann conditions, that is we let the domain move freely in the tangential direction. At the fluid inlet we imposed the patient-specific flow rate depicted in Figure 2, measured by means of the Eco-Color Doppler technique and prescribed through the Lagrange multipliers method (see [15, 46, 18, 19]). At the

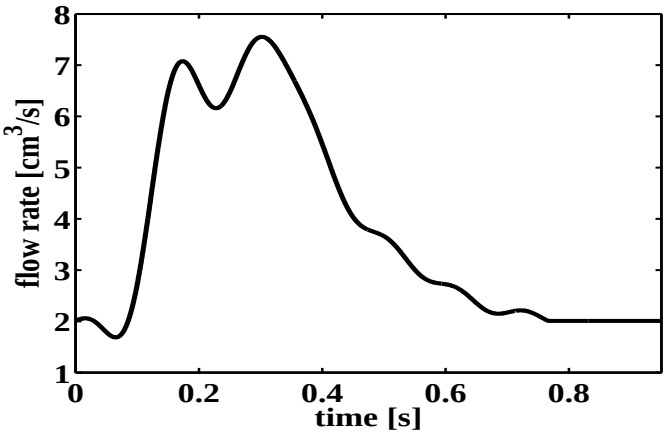

Figure 2: Patient-specific flow rate waveform prescribed at the inlet of the carotid.

fluid outlets, we used an absorbing resistance boundary condition, see [39, 38] for details. At the external surface Σ^0_{out} we prescribed a Robin boundary condition with Robin coefficient α_e with the aim of modeling the presence of a surrounding tissue around the vessel [32, 35, 9, 38]. In particular, we set $\alpha_e = 3 \cdot 10^6\, dyne/cm^3$. This value allows to recover a pressure in the physiological range.

As a representative case, we reported in Figure 3 a snapshot of the streamlines obtained with GC∞-P∞ scheme and BDF1/BDF1 time discretization.

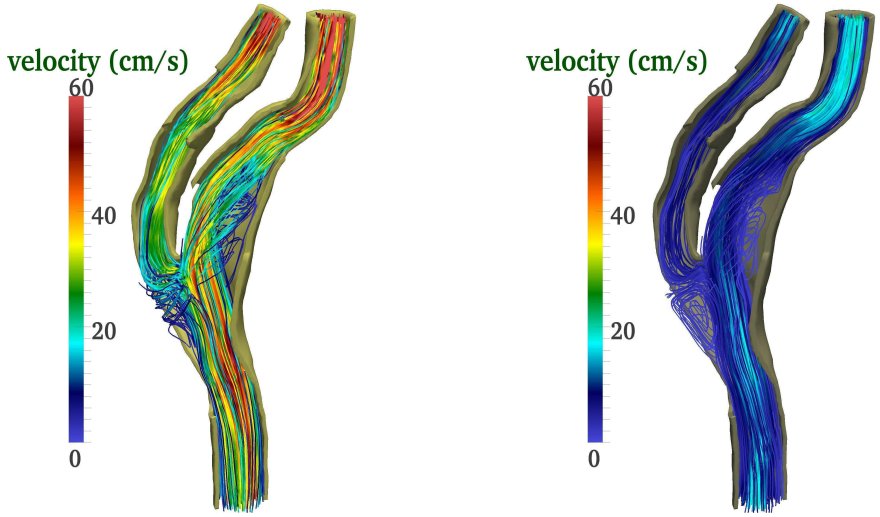

Figure 3: Streamlines of the velocity field at sistole ($0.31\,s$, left) and at diastole ($0.80\,s$, right). GC∞-P∞ - BDF1/BDF1.

In Table 1 we reported the number of iterations for different exact schemes. The number of external iterations reported in the table has to be intended as an average one over the period $[0, T]$, whilst the intermediate and the internal ones as the average per outer loop (the external and the intermediate ones, respectively). We reported also the CPU time normalized over that of GC∞-P∞-DT scheme, used here as our gold-standard.

Discussion of the numerical results. The results reported in Table 1 show that the approximate-Newton-based schemes are the most efficient among exact methods. In particular, GC∞-P∞ scheme is slightly faster than GCP∞. We also ran the proposed numerical experiment with GC∞-P∞-DT scheme, described in Algorithm 3.5. As observed in Table 1, the CPU time needed by GC∞-P∞-DT have been almost halved with respect to GC∞-P∞.

Regarding the fixed-point-based schemes, they seem to be quite slower than approximate-Newton methods. The best performance have been obtained by G∞C∞-P∞ scheme, the CPU time being less than two times greater than for GC∞-P∞. We point out that in any cases, fixed-point-based schemes converged

	# of external iterations	# of intermediate iterations	# of internal iterations	Normalized CPU time
GC∞-P∞	13.5	–	7.7	1.72
GC∞-P∞-DT	13.9	–	3.0	1.00
GCP∞	20.4	–	–	2.00
G∞-CP∞	12.3	–	9.4	3.53
G∞-C∞-P∞	12.3	5.7	6.3	3.05
G∞-P∞-C∞	12.9	6.7	3.5	3.76
GP∞-C∞	15.3	–	3.8	4.16

Table 1: Average number of iterations in the external loop and average number of iterations per outer loop in the intermediate and internal ones, and CPU time normalized with respect to that of GC∞-P∞-DT scheme. Exact schemes. BDF1/BDF1.

without any relaxation ($\omega_G = 1$). We ran G∞-C∞-P∞ scheme also with an Aitken relaxation procedure [26] over (20), with the hope of improving the efficiency. However, we found that the CPU time normalized with respect to that of GC∞-P∞-DT is 2.90, against 3.05 for the case $\omega = 1$, so that no substantial improvement is observed with the Aitken procedure. We did not consider G∞-C∞-P∞-DT scheme, due to the worse performance of G∞-C∞-P∞ with respect to GC∞-P∞.

Concerning the classical schemes, they showed a very poor efficiency in comparison to approximate-Newton, their CPU time being more than four times greater with respect to that of GC∞-P∞-DT. They are also slower than the fixed-point-based methods. Such schemes are however the most appealing from the computational point of view, when one has at disposal two *black-box* solvers for the fluid problem in ALE formulation and for the structure, since they need just to implement suitable routines for the transfer of the interface conditions between the two codes. Instead, approximate-Newton-based and fixed-point-based algorithms can be implemented in a modular way provided that one can access to the fluid and structure tangent problems (always possible by running just 1 Newton internal iteration).

In conclusion, we suggest GC∞-P∞-DT as the most suitable among exact schemes for real haemodynamic applications.

4 Inexact schemes

Here, we want to extend to the case of the finite elasticity the semi-implicit schemes [43, 12, 6, 39, 9] and, more generally, the geometrical inexact schemes [38]. A first way to do this, consists in considering the classical scheme G∞-P∞-C∞ and to perform just one (or few) external iterations over the interface position [35]. In this

case the physical interface conditions and the constitutive non-linearities are both treated exactly. Here, we want to introduce a different family of inexact schemes, where, besides the geometrical interface condition, also the fluid and structure constitutive non-linearities are not prescribed exactly. In other words, we ask if it is necessary in haemodynamic applications to handle exactly the constitutive non-linearities, in particular the structure one. In Section 4.1 we considered the inexact versions of the approximate-Newton-based schemes, and in Section 4.2 the inexact versions of the fixed-point-based schemes. To study the accuracy, we considered both an analytical test case in Section 4.3 and a real test case in Section 4.4. In the latter section, we also study the efficiency of the inexact schemes in a real context.

4.1 Approximate-Newton-based inexact schemes

The starting point is the observation that in the case of the linear infinitesimal elasticity, semi-implicit schemes can be regarded as GC∞-P∞ scheme where the number of external iterations is fixed and equal to 1. By performing just one external iteration also in presence of the finite elasticity, we obtain a scheme where also for the constitutive non-linearities just one iteration is performed (I-GC1-P∞). More in general, it is possible to perform m external iterations for a fixed $m > 1$, obtaining the I-GCm-P∞ scheme. For such schemes, the stopping criteria on the geometrical condition and on the constitutive non-linearities are not checked, so that they are in principle inexact also with respect to the constitutive non-linearities. This fact makes very interesting the study of the accuracy of such schemes, since there is no *a priori* evidence that the fluid and, especially, the structure problems need to be solved exactly in order to recover a global accurate solution.

4.2 Fixed-point-based inexact schemes

We introduce here the inexact variants of the fixed-point-based schemes introduced in Section 3.3. The philosophy is the same used to derive the inexact schemes from the approximate-Newton-based algorithms, that is to perform a fixed number of iterations in the external loops.

We can derive two groups of inexact algorithms, one from G∞-CP∞ scheme and one from G∞-C∞-P∞ scheme. In any case, as for the approximate-Newton-based inexact algorithms, the physical interface conditions are satisfied exactly, due to the high added mass effect in haemodynamics. In the first case we obtain I-Gm-CP∞ schemes, derived from Algorithm 3.3 by performing just m external iterations. This scheme, differently from I-GCm-P∞, solves exactly the constitutive non-linearities, and only the geometrical interface condition is not prescribed correctly. Since we are here interested in the accuracy of schemes which do not solve exactly the constitutive non-linearities, we do not consider such schemes in the following numerical experiments.

The second group of inexact schemes is derived from G∞-C∞-P∞ scheme. In this case, they are obtained by considering just m iterations in the external loop and r iterations in the intermediate loop (in principle, also the case $r = \infty$ could be allowed, but it is not considered here). We obtain I-Gm-Cr-P∞ schemes, derived from Algorithm 3.4 by performing just m external iterations and r intermediate iterations. Such schemes, as for I-GCm-P∞ scheme, treat inexactly both the geometrical interface condition and the constitutive non-linearities.

4.3 Numerical results for inexact schemes: Convergence with respect to time

We consider the same analytical test case proposed in [38] for the linear infinitesimal elasticity. This test consists in a translation of a cylinder of small thickness (the structure) filled by the fluid and in a rotation around its axis with no volume forces.

Referring to the same data reported in [38], it is easy to check that the analytical solution of the FSI problem is given by

$$\begin{cases} \boldsymbol{u}_f = \bar{\boldsymbol{u}} & \text{in } \Omega_f^t, \qquad p_f = 0 \quad \text{in } \Omega_f^t, \\ \widetilde{\boldsymbol{\eta}}_s = \bar{\boldsymbol{\eta}} & \text{in } \Omega_s^0, \qquad \widetilde{\boldsymbol{\eta}}_m = \bar{\boldsymbol{\eta}} \quad \text{in } \Omega_f^0, \end{cases}$$

where

$$\bar{\boldsymbol{\eta}} := \begin{bmatrix} x_{s,1}^0(\cos\theta - 1) - x_{s,2}^0 \sin\theta + c_1, \\ x_{s,1}^0 \sin\theta + x_{s,2}^0(\cos\theta - 1) + c_2, \\ c_3, \end{bmatrix}, \qquad \bar{\boldsymbol{u}} := \begin{bmatrix} \dot{\theta}(c_2 - x_{f,2}) + \dot{c}_1, \\ \dot{\theta}(x_{f,1} - c_1) + \dot{c}_2, \\ \dot{c}_3, \end{bmatrix}$$

for given functions of time $\theta(t)$ and $\boldsymbol{c}(t)$. We observe that with respect to the analytical solution proposed in [38], here the pressure is identically zero.

We considered, in particular, the cylindrical geometry depicted in Figure 4, where the length is $L = 5\,cm$, the fluid domain radius $R = 0.5\,cm$, the structure thickness $H_s = 0.1\,cm$. The space discretization parameter is $h = 0.025\,cm$ and the fluid and structure meshes are conforming at the interface. The mesh is composed of about 57000 degrees of freedom for the fluid and about 6000 for the structure. For what concerns the data of the test, we have set $\boldsymbol{c} = \boldsymbol{0}$ and $\theta(t) = 0.2(1 - cos(50\pi\, t))$. We ran all the simulations on 4 processors for the solution of the fluid problem and on 1 processor for the structure.

In Figure 5 we show the convergence history of four selected inexact schemes, namely I-GC1-P∞, I-GC2-P∞, I-G1-C2-P∞ and I-G2-C2-P∞, chosen as the most representative, for three selected temporal schemes, namely BDF1/BDF1, BDF2/BDF2 and BDF3/BDF3. A relative L^2 norm of the error is computed at time $t = 0.002\,s$. The time discretization parameter is $\Delta t = 2 \cdot 10^{-3}$, 10^{-3}, $5 \cdot 10^{-4}$, $2.5 \cdot 10^{-4}\,s$. For BDF2/BDF2 and BDF3/BDF3 schemes, I-GC1-P∞ and I-G1-C2-P∞ featured just first order convergence, so that we have considered in these cases also the extrapolated versions I-GC1E-P∞ and I-G1E-C2-P∞.

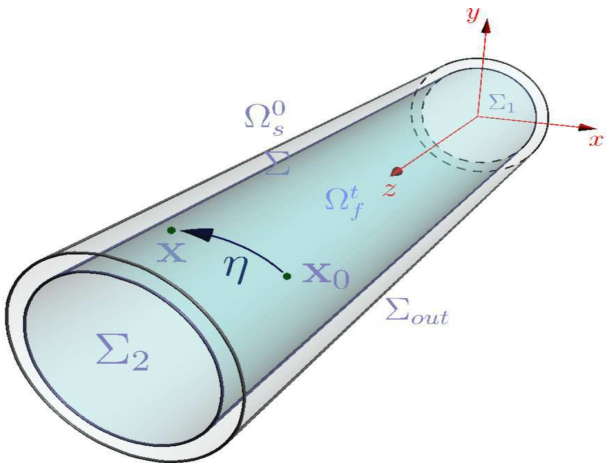

Figure 4: Cylindrical geometry.

Discussion of the numerical results. From the convergence rates depicted in Figure 5, we observe that when BDF1/BDF1 is used, all the four inexact schemes considered recovered first order convergence without any extrapolation of the interface position, fluid velocity and structure displacement. Regarding BDF2/BDF2 and BDF3/BDF3, we observe that schemes which perform two iterations in the loops related to the geometrical condition and to the constitutive non-linearities (I-GC2-P∞ and I-G2-C2-P∞) featured second and third order convergence, respectively, without any extrapolation. For the other two schemes (I-GC1E-P∞ and I-G1E-C2-P∞) an extrapolation of order two and three, respectively, has been needed in order to recover the right convergence order. This results show that, at least for the analytical test case, it is not needed to solve exactly the constitutive non-linearities to recover an accurate solution.

4.4 Numerical results for inexact schemes: Efficiency and accuracy in a real test case

In this section we report the numerical results obtained for the same test case presented in Section 3.5.2, by using the four inexact schemes considered above. This allowed to study the accuracy and the efficiency of such schemes in a real context.

In Tables 2 and 3 we report the relative errors of the inexact schemes by using the solution obtained with GC∞-P∞ scheme as the reference one. In particular, we report the $L^\infty(L^\infty)$-norm of average quantities, namely the mean structure displacement η, the flow rate Q and the mean pressure P computed over sections

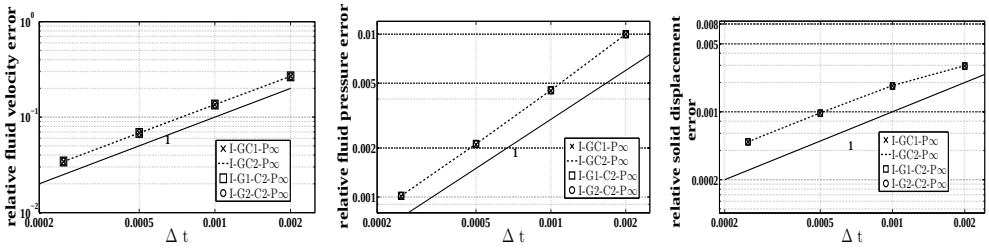

(a) BDF1/BDF1

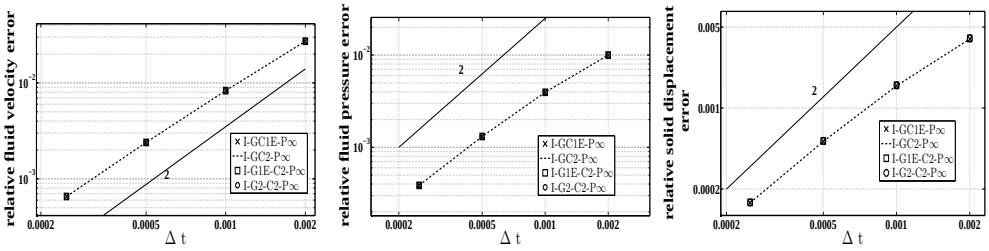

(b) BDF2/BDF2

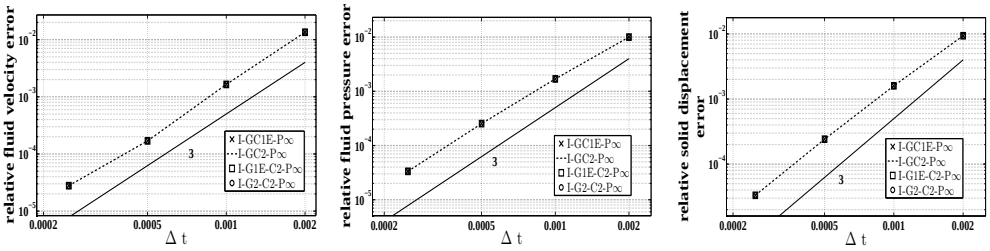

(c) BDF3/BDF3

Figure 5: Convergence rate of three temporal schemes considered. Relative errors of the fluid velocity (left), of the pressure (middle) and of the structure displacement (right) - BDF1/BDF1 (up), BDF2/BDF2 (middle), BDF3/BDF3 (bottom) - $t = 0.002\,s$.

perpendicular to the axial axis. To do this, we computed quantities as

$$\frac{\max_j \|x^j_{EX} - x^j_*\|_{L^\infty(0,T)}}{\max_j \|x^j_{EX}\|_{L^\infty(0,T)}}, \tag{26}$$

where x^j is one of the average quantities computed at different sections Σ_j orthogonal to the axial direction, EX stands for "solution computed with the exact

scheme" and * stands for one of the inexact schemes. The results reported in Table 2 refer to BDF1/BDF1, while those in Table 3 to BDF2/BDF2.

	η (%)	Q (%)	P(%)
I-GC1-P∞	0.890	0.413	0.702
I-GC2-P∞	0.003	0.005	0.003
I-G1-C2-P∞	0.847	0.439	0.694
I-G2-C2-P∞	0.002	0.001	0.001

Table 2: Relative error of inexact schemes with respect to the exact solution, computed with (26). BDF1/BDF1. Left: displacement. Middle: flow rate. Right: mean pressure.

	η (%)	Q (%)	P(%)
I-GC1-P∞	1.013	0.832	1.342
I-GC1E-P∞	0.066	0.084	0.054
I-GC2-P∞	0.004	0.006	0.004
I-G1-C2-P∞	0.994	0.768	0.078
I-G1E-C2-P∞	0.042	0.027	0.025
I-G2-C2-P∞	0.003	0.002	0.002

Table 3: Relative error of inexact schemes with respect to the exact solution, computed with (26). BDF2/BDF2. Left: displacement. Middle: flow rate. Right: mean pressure.

In Table 4 we report the number of iterations for BDF2/BDF2. In particular, the number of iterations in the intermediate and in the internal loops has to be intended as the average per outer loop. We also report the CPU time normalized over that of GC∞-P∞-DT scheme, that is the fastest among the exact schemes.

Discussion of the numerical results. The results reported in Tables 2 and 3 show that the relative errors of inexact schemes with respect to the solution obtained with an exact scheme are in any case less than 1%. In particular, the accuracy improves of one order of magnitude by performing just one external iteration with a suitable extrapolation in the case of BDF2/BDF2, and of two orders of magnitude by performing two external iterations instead of one both for BDF1/BDF1 and for BDF2/BDF2, These results show that also in real applications, an inexact treatment of the constitutive non-linearities and of the geometrical interface condition is sufficient to recover a satisfactory solution for practical purposes.

Regarding the efficiency, we observed that the inexact approximate-Newton-based methods are slightly faster than the inexact fixed-point-based ones, while

	# of external iterations	# of intermediate iterations	# of internal iterations	Normalized CPU time
I-GC1-P∞	1	–	24.8	0.34
I-GC1E-P∞	1	–	24.6	0.33
I-GC2-P∞	2	–	20.3	0.70
I-G1-C2-P∞	1	2	21.8	0.46
I-G1E-C2-P∞	1	2	21.4	0.44
I-G2-C2-P∞	2	2	18.6	0.83

Table 4: Average number of iterations per outer loop in the intermediate and internal ones, and CPU time normalized with respect to that of GC∞-P∞-DT scheme. Inexact schemes. BDF2/BDF2.

we did not experience significant differences in the case of one external iteration between the cases with or without extrapolation, see Table 4. Performing just one external iteration allows a big saving in the computational effort, being the CPU times reduced to three times. When moving from one to two external iterations, the CPU time doubles, being however less than the CPU time of the most efficient exact schemes.

5 Conclusions

In this work we studied the numerical performance of several partitioned schemes for the solutions of the FSI problem with non-linear fluid and structure subproblems for real haemodynamic applications. We considered approximate-Newton-based, fixed-point-based and classical methods. For the first two families of schemes, we considered both exact and inexact schemes, the latter being obtained by performing just one or two iterations in the loops managing the geometrical coupling and the constitutive non-linearities, guaranteeing in any case the satisfaction of the physical interface conditions. The main features of such schemes highlighted by this work are summarized as follows.

1. Among exact schemes, approximate-Newton methods are in general more performing than fixed-point ones. In particular, GC∞-P∞ is the most efficient for real applications;

2. For the latter scheme, we also experienced the excellent performance of a variant where the physical interface conditions in the internal loop are solved with a precision which is proportional to the external residual (GC∞-P∞-DT). This scheme allowed to almost half the CPU times with respect to GC∞-P∞;

3. Classical schemes are more than four times slower than approximate-Newton

methods, being however the easier to be implemented when black-box solvers are available;

4. Inexact schemes, where both the geometrical interface condition and the constitutive non-linearities are not prescribed exactly, are accurate, recovering, for the analytical test case, the expected convergence rate when at most two iterations involved in the relative loops are performed. When just one iteration is considered, a suitable extrapolation of interface position, fluid velocity and structure displacement is needed to recover the right order of convergence.

5. Inexact schemes, where two iterations in the external loops are performed are very accurate for real haemodynamic applications. A very good accuracy (even if worse than that obtained with two external iterations) has been experienced also when performing one external iteration for BDF2/BDF2, provided that a suitable extrapolation is considered. These facts confirm, for the first time, the effectiveness of inexact schemes in haemodynamics also when the finite elasticity is considered for the structure subproblem;

6. Inexact schemes are more efficient than exact schemes, the CPU time being reduced to three times when just one external iteration is performed.

For the reasons highlighted at the previous points, among all the schemes proposed in this work, we recommend I-GC2-P∞ as the best compromise between good accuracy and efficiency for real haemodynamic applications. For BDF2/BDF2 an effective alternative is provided by I-GC1E-P∞, which allows to half the CPU times with respect to I-GC2-P∞, with a slight reduction in the accuracy (the errors being however less than 0.1%).

Acknowledgments

The numerical simulations have been performed at CILEA Consortium through a LISA Initiative (Laboratory for Interdisciplinary Advanced Simulation) 2012 grant [link:http://lisa.cilea.it]. The authors would like to thank M. Domanin, L. Forzenigo and P. Biondetti, which have provided the patient images, and L. Azzimonti and P. Secchi, which have provided the patient-specific flow waveform depicted in Figure 2 from Eco-color Doppler analysis.

References

[1] M. Astorino, F. Chouly, and M. Fernández, *Robin based semi-implicit coupling in fluid-structure interaction: stability analysis and numerics*, SIAM J. Sci. Comp., 31 (2009), pp. 4041–4065.

[2] M. Astorino and C. Grandmont, *Convergence analysis of a projection semi-implicit coupling scheme for fluid-structure interaction problems*, Numer Math, (2010), pp. 721–767.

[3] S. Badia, F. Nobile, and C. Vergara, *Fluid-structure partitioned procedures based on Robin transmission conditions*, J. Comput. Physics, 227 (2008), pp. 7027–7051.

[4] ——, *Robin-Robin preconditioned Krylov methods for fluid-structure interaction problems*, Comput. Methods Appl. Mech. Engrg., 198 (2009), pp. 2768–2784.

[5] S. Badia, A. Quaini, and A. Quarteroni, *Modular vs. non-modular preconditioners for fluid-structure systems with large added-mass effect*, Comput. Methods Appl. Mech. Engrg., 197 (2008), pp. 4216–4232.

[6] ——, *Splitting methods based on algebraic factorization for fluid-structure interaction*, SIAM J. Sci. Comp., 30 (2008), pp. 1778–1805.

[7] Y. Bazilevs, V. Calo, Y. Zhang, and T. Hughes, *Isogeometric fluid-structure interaction analysis with applications to arterial blood flow.*, Computational Mechanics, 38 (2006), pp. 310–322.

[8] P. Causin, J. Gerbeau, and F. Nobile, *Added-mass effect in the design of partitioned algorithms for fluid-structure problems*, Comput. Methods Appl. Mech. Engrg., 194(42-44) (2005), pp. 4506–4527.

[9] P. Crosetto, S. Deparis, G. Fourestey, and A. Quarteroni, *Parallel algorithms for fluid-structure interaction problems in haemodynamics*, SIAM J. Sci. Comp., 33(4) (2011), pp. 1598–1622.

[10] W. Dettmer and D. Perić, *On the coupling between fluid flow and mesh motion in the modelling of fluid-structure interaction*, Comp. Mech., 43 (2008), pp. 81–90.

[11] J. Donea, *An arbitrary Lagrangian-Eulerian finite element method for transient dynamic fluid-structure interaction*, Comput. Methods Appl. Mech. Engrg., 33 (1982), pp. 689–723.

[12] M. Fernández, J. Gerbeau, and C. Grandmont, *A projection semi-implicit scheme for the coupling of an elastic structure with an incompressible fluid*, Int. J. Num. Methods Engrg., 69 (2007), pp. 794–821.

[13] M. Fernández and M. Moubachir, *A Newton method using exact Jacobians for solving fluid-structure coupling*, Computers & Structures, 83(2-3) (2005), pp. 127–142.

[14] C. Figueroa, I. Vignon-Clementel, K. Jansen, T. Hughes, and C. Taylor, *A coupled momentum method for modeling blood flow in three-dimensional deformable arteries*, Comput. Methods Appl. Mech. Engrg., 195 (2006), pp. 5685–5706.

[15] L. Formaggia, J.-F. Gerbeau, F. Nobile, and A. Quarteroni, *Numerical treatment of defective boundary conditions for the Navier-Stokes equation*, SIAM J. Numer. Anal., 40(1) (2002), pp. 376–401.

[16] L. Formaggia, A. Quarteroni, and A. Veneziani (eds), *Cardiovascular Mathematics - Modeling and simulation of the circulatory system*, Springer, 2009.

[17] L. Formaggia, A. Quarteroni, and C. Vergara, *On the physical consistency between three-dimensional and one-dimensional models in haemodynamics.*, J. Comput. Physics, DOI:10.1016/j.jcp.2012.08.001 (2012).

[18] L. Formaggia, A. Veneziani, and C. Vergara, *Flow rate boundary problems for an incompressible fluid in deformable domains: formulations and solution methods*, Comput. Methods Appl. Mech. Engrg., 199 (9-12) (2009), pp. 677–688.

[19] L. Formaggia and C. Vergara, *Prescription of general defective boundary conditions in fluid-dynamics*, Milan Journal of Mathematics, DOI:10.1007/s00032-012-0185-8 (2012).

[20] C. Forster, W. Wall, and E. Ramm, *Artificial added mass instabilities in sequential staggered coupling of nonlinear structures and incompressible viscous flow*, Comput. Methods Appl. Mech. Engrg., 196 (2007), pp. 1278–1293.

[21] M. Gee, U. Kuttler, and W. Wall, *Truly monolithic algebraic multigrid for fluid-structure interaction*, Int. J. Num. Methods Engrg., 85(8) (2011), pp. 987–1016.

[22] L. Gerardo Giorda, F. Nobile, and C. Vergara, *Analysis and optimization of Robin-Robin partitioned procedures in fluid-structure interaction problems*, SIAM J. Numer. Anal., 48(6) (2010), pp. 2091–2116.

[23] M. Heil, *An efficient solver for the fully coupled solution of large-displacement fluid-structure interaction problems*, Comput. Methods Appl. Mech. Engrg., 193 (2004), pp. 1–23.

[24] M. Heil, A. Hazel, and J. Boyle, *Solvers for large-displacement fluidstructure interaction problems: segregated versus monolithic approaches*, Comp. Mech., 43(1) (2008), pp. 91–101.

[25] T. J. R. Hughes, W. K. Liu, and T. K. Zimmermann, *Lagrangian-Eulerian finite element formulation for incompressible viscous flows*, Comput. Methods Appl. Mech. Engrg., 29 (1981), pp. 329–349.

[26] B. Irons and R.C.Tuck, *A version of the Aitken accelerator for computer implementation*, Int. J. Num. Methods Engrg., 1 (1969), pp. 275–277.

[27] C. Kassiotis, A. Ibrahimbegovic, R. Niekamp, and H. Matthies, *Nonlinear fluid-structure interaction problem. part i: implicit partitioned algorithm, nonlinear stability proof and validation examples*, Comput. Mech., 47 (2011), pp. 305–323.

[28] C. Kelley, *Iterative methods for linear and non-linear equations*, SIAM, 1995.

[29] R. Kirby, Z. Yosibash, and G. Karniadakis, *Towards stable coupling methods for high-order discretization of fluid-structure interaction: Algorithms and observations*, J. Comput. Physics, 223 (2007), pp. 489–518.

[30] U. Kuttler, M. Gee, C. Forster, A. Comerford, and W. Wall, *Coupling strategies for biomedical fluid-structure interaction problems*, Int. J. Num. Methods Biomed. Engrg., 26 (2010), pp. 305–321.

[31] U. Kuttler and W. Wall, *Fixed-point fluid-structure interaction solvers with dynamic relaxation*, Comput. Mech., 43 (2008), pp. 61–72.

[32] Y. Liu, C. Charles, M. Gracia, H. Gregersen, and G. S. Kassab, *Surrounding tissues affect the passive mechanics of the vessel wall: theory and experiment*, Am. J. Physiol. Heart Circ. Physiol., 293 (2007), pp. H3290–H3300.

[33] H. Matthies, R. Niekamp, and J. Steindorf, *Algorithms for strong coupling procedures*, Computers & Structures, 195 (2006), pp. 2028–2049.

[34] G. Mengaldo, P. Tricerri, P. Crosetto, S. Deparis, F. Nobile, and L. Formaggia, *A comparative study of different nonlinear hyperelastic isotropic arterial wall models in patient-specific vascular flow simulations in the aortic arch*, MOX-Report n. 15-2012, Department of Mathematics, Politecnico di Milano, Italy, 2012.

[35] P. Moireau, N. Xiao, M. Astorino, C. A. Figueroa, D. Chapelle, C. A. Taylor, and J.-F. Gerbeau, *External tissue support and fluidstructure simulation in blood flows*, Biomechanics and Modeling in Mechanobiology, 11(1-2) (2012), pp. 1–18.

[36] C. M. Murea and S. Sy, *A fast method for solving fluid-structure interaction problems numerically*, Int. J. Num. Methods Fluids, 60 (2009), pp. 1149–1172.

[37] F. Nobile, *Numerical approximation of fluid-structure interaction problems with application to haemodynamics*, PhD thesis, École Polytechnique Fédérale de Lausanne, 2001. Thesis n° 2458.

[38] F. Nobile, M. Pozzoli, and C. Vergara, *Time accurate partitioned algorithms for the solution of fluid-structure interaction problems in haemodynamics*, MOX-Report n. 30-2011, Department of Mathematics, Politecnico di Milano, Italy, 2011.

[39] F. Nobile and C. Vergara, *An effective fluid-structure interaction formulation for vascular dynamics by generalized Robin conditions*, SIAM J. Sci. Comp., 30 (2008), pp. 731–763.

[40] ——, *Partitioned algorithms for fluid-structure interaction problems in haemodynamics*, MOX-Report n. 23-2012, Department of Mathematics, Politecnico di Milano, Italy, 2011.

[41] K. Perktold, E. Thurner, and T. Kenner, *Flow and stress characteristics in rigid walled and compliant carotid artery bifurcation models*, Medical and Biological Engineering and Computing, 32 (1994), pp. 19–26.

[42] M. Pozzoli, *Efficient partitioned algorithms for the solution of fluid-structure interaction problems in haemodynamics*, PhD thesis, Politecnico di Milano, Febrary 2012. Academic year: XXIV.

[43] E. Swim and P. Seshaiyer, *A nonconforming finite element method for fluid-structure interaction problems*, Comput. Methods Appl. Mech. Engrg., (2006), pp. 2088–2099.

[44] T. Tezduyar, S. Sathe, T. Cragin, B. Nanna, B. Conklin, J. Pausewang, and M. Schwaab, *Modelling of fluid-structure interactions with the space-time finite elements: arterial fluid mechanics*, Int. J. Num. Methods Fluids, 54 (2007), pp. 901–922.

[45] T. Tezduyar, S. Sathe, and K. Stein, *Solution techniques for the fully discretized equations in computation of fluidstructure interactions with the spacetime formulations*, Comput. Methods Appl. Mech. Engrg., 195(41-43) (2006), p. 57435753.

[46] A. Veneziani and C. Vergara, *Flow rate defective boundary conditions in haemodinamics simulations*, Int. J. Num. Methods Fluids, 47 (2005), pp. 803–816.

MOX Technical Reports, last issues

Dipartimento di Matematica "F. Brioschi",
Politecnico di Milano, Via Bonardi 9 - 20133 Milano (Italy)

39/2012 Ieva, F.; Paganoni, A.M.; Ziller, S.
Operational risk management: a statistical perspective

38/2012 Antonietti, P.F.; Bigoni, N.; Verani, M.
Mimetic finite difference approximation of quasilinear elliptic problems

37/2012 Nobile, F.; Pozzoli, M.; Vergara, C.
Exact and inexact partitioned algorithms for fluid-structure interaction problems with finite elasticity in haemodynamics

36/2012 Canuto, C.; Verani, M.
On the Numerical Analysis of Adaptive Spectral/hp Methods for Elliptic Problems

35/2012 Pigoli, D.; Aston, J.A.D.; Dryden, I.L.; Secchi, P.
Distances and Inference for Covariance Functions

34/2012 Menafoglio, A.; Dalla Rosa, M.; Secchi, P.
A Universal Kriging predictor for spatially dependent functional data of a Hilbert Space

33/2012 Motamed, M.; Nobile, F.; Tempone, R.
Analysis and computation of the elastic wave equation with random coefficients

32/2012 Formaggia, L.; Fumagalli, A.; Scotti A.; Ruffo, P
A reduced model for Darcy s problem in networks of fractures

31/2012 Bonizzoni, F.; Buffa, A; Nobile, F:
Moment equations for the mixed formulation of the Hodge Laplacian with stochastic data

30/2012 Beck, J.; Nobile, F.; Tamellini, L.; Tempone, R.;
Convergence of quasi-optimal Stochastic Galerkin Methods for a class of PDES with random coefficients